

1 Quasi-consistent efficient meshfree thin shell
2 formulation ~~to naturally accommodate~~with penalty-free
3 essential boundary ~~conditions~~condition enforcement

4 Junchao Wu^{a,*}, Yangtao Xu^a, Bin Xu^a, Syed Humayun Basha^a

^a*Key Laboratory for Intelligent Infrastructure and Monitoring of Fujian Province, Key Laboratory for Structural Engineering and Disaster Prevention of Fujian Province, College of Civil Engineering, Huaqiao University, Xiamen, Fujian, 361021, China*

5 **Abstract**

This research proposed an efficient and quasi-consistent meshfree thin shell formulation with ~~natural~~penalty-free enforcement of essential boundary conditions. Within the framework of the Hu-Washizu variational principle, a mixed formulation of displacements, strains and stresses is employed in this approach, where the displacements are discretized using meshfree shape functions, and the strains and stresses are expressed using smoothed gradients, covariant smoothed gradients and covariant bases. The smoothed gradients satisfy the first ~~and second order~~second-order integration constraint and have ~~quasi-consistent consistency~~variational consistency for polynomial strains and stresses. Owing to Hu-Washizu variational principle, the essential boundary conditions automatically arise in its weak form. As a result, the suggested technique's enforcement of essential boundary conditions resembles that of the traditional Nitsche's method. Contrary to Nitsche's method, the costly higher order derivatives of conventional meshfree shape functions were replaced by the smoothed gradients with fast computation, which improve the efficiency. Meanwhile, the proposed formulation features a naturally stabilized term without adding any artificial stabilization factors, which eliminates the ~~stabilization parameter-dependent issue in the Nitsche's method~~employment of penalty method as a stabilization. The efficacy of the proposed Hu-Washizu meshfree thin shell formulation is illustrated by a set of classical standard thin shell problems.

6 **Keywords:** Meshfree, Thin shell, Hu-Washizu variational principle,
7 Reproducing kernel gradient smoothing, Essential boundary condition

*Corresponding author
Email address: jcwu@hqu.edu.cn (Junchao Wu)

8 1. Introduction

9 Thin shell structures generally adhere to the Kirchhoff hypothesis [1], that
10 neglects the shear deformation can be described using Galerkin formulation
11 which requires to have at least C^1 continuity. The traditional finite element
12 methods usually only have C^0 continuous shape functions, and it prefers Mindlin
13 thick shear theory, hybrid and mixed models in simulation of shell structure [2].
14 Meshfree methods [3, 4, 5] with high order smoothed shape functions have gar-
15 nered much research attention over the past thirty years. These techniques
16 established the shape functions based on a collection of dispersed nodes, and
17 the high order continuity of shape functions can be easily achieved even with
18 low-order basis functions. For thin shell analysis, this high order meshfree ap-
19 proximation can also alleviate the membrane locking caused by the mismatched
20 approximation order of membrane strain and bending strain [6]. Furthermore,
21 nodal-based meshfree approximations generally offer the flexibility of local re-
22 finement and can relieve the burden of mesh distortion. Owing to these benefits,
23 numerous meshfree techniques have been developed and implemented in many
24 scientific and engineering fields [7, 8, 9, 10, 11, 12, 13]. However,
25 the high order smoothed meshfree shape functions accompany the enlarged and
26 overlapping supports, which may potentially cause many problems for shape
27 functions. One of the issues is the loss of the Kronecker delta property, which
28 means that, unlike the finite element methods, the necessary boundary con-
29 ditions cannot be directly enforced [14]. Another issue is that the variational
30 consistency or said integration constraint, which is a condition requires the
31 formulation to exactly reproduce the solution spanned by basis functions, can-
32 not be satisfied due to. This issue is caused by the misalignment between the
33 numerical integration domains and supports of shape functions. Besides, and
34 thus, the shape functions exhibit a piecewise rational to a piecewise nature in
35 each integration domain. It turns to that the traditional integration rules like
36 Gauss scheme cannot ensure the integration accuracy in Galerkin weak form
37 [15, 16]. Therefore, variational consistency is vital to the solution accuracy in
38 Galerkin formulations [15, 16].

39 Various ways have been presented to enforce the necessary boundary for
40 Galerkin meshfree methods directly, including the boundary singular kernel
41 method [17], mixed transformation method [17], and interpolation element-free
42 method [18] for recovering shape functions' Kronecker property. However, these
43 methods are not based on a variational setting and cannot guarantee varia-
44 tional consistency. In the absence of a meshfree node, accuracy enforcement
45 might be poorer. In contrast, enforcing the essential boundary conditions using
46 a variational approach is preferred for Galerkin meshfree methods. The varia-
47 tional consistent Lagrange multiplier approach was initially used to the Galerkin
48 meshfree method by Belytschko et al. [3]. In this method, the extra degrees
49 of freedom are used to determine the discretion of Lagrange multiplier. Fur-
50 thermore, Ivannikov et al. [19] have extended this approach to geometrically
51 nonlinear thin shells. Lu et al. [20] suggested the modified variational es-
52 sential boundary enforcement approach and expressed the Lagrange multiplier

53 by equivalent tractions to eliminate the excess degrees of freedom. However,
54 the coercivity of this approach is not always ensured and potentially reduces
55 the accuracy. Zhu and Atluri [21] pioneered the penalty method for meshfree
56 method, making it a straightforward approach to enforce essential boundary
57 conditions via Galerkin weak form. However, the penalty method lacks varia-
58 tional consistency and requires experimental artificial parameters whose optimal
59 value is hard to determine. Fernández-Méndez and Huerta [14] imposed neces-
60 sary boundary conditions using Nitsche's approach in the meshfree formulation.
61 This approach can be seen as a hybrid combination of the modified variational
62 method and the penalty method because the modified variational method gen-
63 erates variational consistency through the use of a consistent term, and the
64 penalty method is used as a stabilized term to recover the coercivity. Skatulla
65 and Sansour [22] extended Nitsche's thin shell analysis method and proposed an
66 iteration algorithm to determine artificial parameters at each integration point.

67 In order to address the issue of numerical integration, a series of consis-
68 tent integration schemes have been developed for Galerkin meshfree methods.
69 Among these include stabilized conforming nodal integration [23], variational
70 consistent integration [24], quadratic consistent integration [25], reproducing
71 kernel gradient smoothing integration [26], and consistent projection integration
72 [27]. The assumed strain approach establishes the most consistent integration
73 scheme, while the smoothed gradient replaces the costly higher order derivatives
74 of traditional meshfree shape functions and shows a high efficiency. Moreover,
75 to achieve global variational consistency, a consistent essential boundary con-
76 dition enforcement should cooperate with the consistent integration scheme.
77 The consistent integration scheme and Nitsche's method for treating essential
78 boundary conditions show a good performance since they can satisfy the coer-
79 civity without requiring additional degrees of freedom. Nevertheless, Nitsche's
80 approach still retains the artificial parameters in stabilized terms, and it is es-
81 sential to remain conscious of the costly higher order derivatives, particularly
82 for thin plate and thin shell problems. Recently, Wu et al. [28, 29] proposed
83 an efficient and stabilized essential boundary condition enforcement method
84 based upon the Hellinger-Reissner variational principle, where a mixed formu-
85 lation in Hellinger-Reissner weak form recasts the reproducing kernel gradient
86 smoothing integration. The terms for enforcing essential boundary conditions
87 are identical to the Nitsche's method, and both have consistent and stabilized
88 terms. Nevertheless, the stabilized term of this method naturally exists in the
89 Hellinger-Reissner weak form and no longer needs the artificial parameters, even
90 for essential boundary enforcement; instead all of the higher order derivatives
91 are represented by smoothed gradients and their derivatives.

92 In this study, an efficient and stabilized variational consistent meshfree
93 method that naturally enforces the essential boundary conditions is developed
94 for thin shell structure. Following the concept of the Hellinger-Reissner prin-
95 ciple base consistent meshfree method, the Hu-Washizu variational principle of
96 complementary energy with variables of displacement, strains, and stresses is
97 employed. The displacement is approximated by conventional meshfree shape
98 functions, and the strains and stresses are expressed by smoothed gradients with

99 covariant bases. It is important to note that although the first second-order in-
100 tegration requirements are naturally embedded in the smoothed gradients, their
101 fulfillment can only result in a quasi-satisfaction of variational consistency be-
102 cause of the non-polynomial nature of the stresses. Hu-Washizu's weak form is
103 used to evaluate all the essential boundary conditions regarding displacements
104 and rotations. This type of formulation is similar to the Nitsche's method but
105 does not require any artificial parameters. Compared with Nitsche's method,
106 conventional reproducing smoothed gradients and its direct derivatives replace
107 the costly higher order derivatives. By utilizing the advantages of a replicating
108 kernel gradient smoothing framework, the smoothed gradients showed better
109 performance compared to conventional derivatives of shape functions, hence
110 increasing the meshfree formulation's computational efficiency.

111 The remainder of this research paper is structured as follows: The kinematics
112 of the thin shell structure and the weak form of the associated Hu-Washizu
113 principle are briefly described in Section 2. Subsequently, the mixed formulation
114 regarding the displacements, strains and stresses in accordance with Hu-Washizu
115 weak form are presented in Section 3. The discrete equilibrium equations are
116 derived in Section 4 using the naturally occurring accommodation of essential,
117 and they are compared to the equations obtained using Nitsche's method. The
118 numerical results in Section 5 validate the efficacy of the proposed Hu-Washizu
119 meshfree thin shell formulation. Lastly, the concluding remarks are presented
120 in Section 6.

121 **2. Hu-Washizu's formulation of complementary energy for thin shell**

122 *2.1. Kinematics for thin shell*

123 Consider the configuration of a shell $\bar{\Omega}$, as shown in Fig. 1, which can be
 124 easily described by a parametric curvilinear coordinate system $\xi = \{\xi^i\}_{i=1,2,3}$.
 125 The mid-surface of the shell denoted by Ω is specified by the in-plane coordinates
 126 $\xi = \{\xi^\alpha\}_{\alpha=1,2}$, as the thickness direction of shell is by ξ^3 , $-\frac{h}{2} \leq \xi^3 \leq \frac{h}{2}$, h is
 127 the thickness of shell. In this work, Latin indices take the values from 1 to 3,
 128 and Greek indices are evaluated by 1 or 2. For the Kirchhoff hypothesis [6], the
 129 position $\mathbf{x} \in \bar{\Omega}$ is defined by linear functions with respect to ξ^3 :

$$\mathbf{x}(\xi^1, \xi^2, \xi^3) = \mathbf{r}(\xi^1, \xi^2) + \xi^3 \mathbf{a}_3(\xi^1, \xi^2) \quad (1)$$

in which \mathbf{r} means the position on the mid-surface of shell, and \mathbf{a}_3 is correspond-

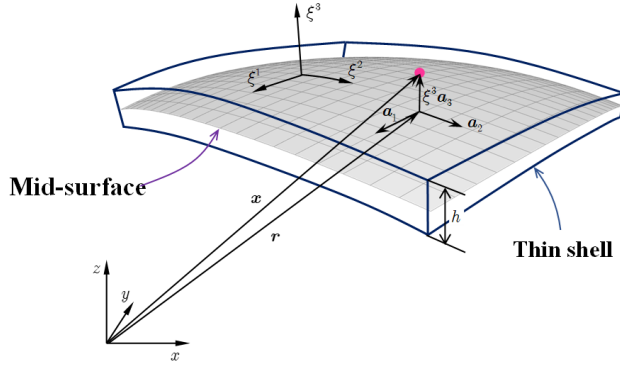


Figure 1: Kinematics for thin shell.

130
 131 ing normal direction. For the mid-surface of shell, the in-plane covariant base
 132 vector with respect to ξ^α can be derived by a trivial partial differentiation to \mathbf{r} :

$$\mathbf{a}_\alpha = \frac{\partial \mathbf{r}}{\partial \xi^\alpha} = \mathbf{r}_{,\alpha}, \alpha = 1, 2 \quad (2)$$

133 to provide for a clear expression, the subscript comma denotes the partial dif-
 134 ferentiation operation with respect to in-plane coordinates ξ^α , and the normal
 135 vector \mathbf{a}_3 can be obtained by the normalized cross product of \mathbf{a}_α 's as follows:

$$\mathbf{a}_3 = \frac{\mathbf{a}_1 \times \mathbf{a}_2}{\|\mathbf{a}_1 \times \mathbf{a}_2\|} \quad (3)$$

136 where $\|\bullet\|$ is the Euclidean norm operator.

137 With the assumption of infinitesimal deformation, the strain components
 138 with respect to the global contravariant base can be stated as:

$$\epsilon_{ij} = \frac{1}{2} (\mathbf{x}_{,i} \cdot \mathbf{u}_{,j} + \mathbf{u}_{,i} \cdot \mathbf{x}_{,j}) \quad (4)$$

¹³⁹ where \mathbf{u} represents the displacement for the shell deformation. To satisfy the
¹⁴⁰ Kirchhoff hypothesis, the displacement is assumed to be of the following form:

$$\mathbf{u}(\xi^1, \xi^2, \xi^3) = \mathbf{v}(\xi^1, \xi^2) + \boldsymbol{\theta}(\xi^1, \xi^2)\xi^3 \quad (5)$$

¹⁴¹ in which the quadratic and higher order terms are neglected. $\mathbf{v}, \boldsymbol{\theta}$ represent
¹⁴² the displacement and rotation in mid-surface, respectively.

¹⁴³ Subsequently, plugging Eqs. (1) and (5) into Eq. (4) and neglecting the
¹⁴⁴ quadratic terms, the strain components can be rephrased as follows:

$$\begin{aligned} \epsilon_{\alpha\beta} &= \frac{1}{2}(\mathbf{a}_\alpha \cdot \mathbf{v}_{,\beta} + \mathbf{v}_{,\alpha} \cdot \mathbf{a}_\beta) \\ &\quad + \frac{1}{2}(\mathbf{a}_{3,\alpha} \cdot \mathbf{v}_{,\beta} + \mathbf{v}_{,\alpha} \cdot \mathbf{a}_{3,\beta} + \mathbf{a}_\alpha \cdot \boldsymbol{\theta}_{,\beta} + \boldsymbol{\theta}_{,\alpha} \cdot \mathbf{a}_\beta)\xi^3 \end{aligned} \quad (6a)$$

$$\epsilon_{\alpha 3} = \frac{1}{2}(\mathbf{a}_\alpha \cdot \boldsymbol{\theta} + \mathbf{v}_{,\alpha} \cdot \mathbf{a}_3) + \frac{1}{2}(\mathbf{a}_3 \cdot \boldsymbol{\theta})_{,\alpha}\xi^3 \quad (6b)$$

$$\epsilon_{33} = \mathbf{a}_3 \cdot \boldsymbol{\theta} \quad (6c)$$

¹⁴⁵ where $\epsilon_{\alpha\beta}, \kappa_{\alpha\beta}$ represent membrane and bending strains, respectively, and are
¹⁴⁶ given as follows:

$$\epsilon_{\alpha\beta} = \frac{1}{2}(\mathbf{a}_\alpha \cdot \mathbf{v}_{,\beta} + \mathbf{v}_{,\alpha} \cdot \mathbf{a}_\beta) \quad (7)$$

$$\kappa_{\alpha\beta} = \frac{1}{2}(\mathbf{a}_{3,\alpha} \cdot \mathbf{v}_{,\beta} + \mathbf{v}_{,\alpha} \cdot \mathbf{a}_{3,\beta} + \mathbf{a}_\alpha \cdot \boldsymbol{\theta}_{,\beta} + \boldsymbol{\theta}_{,\alpha} \cdot \mathbf{a}_\beta) \quad (8)$$

¹⁴⁸ In accordance with the Kirchhoff hypothesis, the thickness of shell will not
¹⁴⁹ change, and the deformation related with direction of ξ^3 will vanish, i.e. $\epsilon_{3i} = 0$.
¹⁵⁰ Thus, the rotation $\boldsymbol{\theta}$ can be rewritten as:

$$\epsilon_{3i} = 0 \Rightarrow \begin{cases} \boldsymbol{\theta} \cdot \mathbf{a}_\alpha \cancel{+} \cancel{-} \mathbf{v}_{,\alpha} \cdot \mathbf{a}_3 = 0 \\ \boldsymbol{\theta} \cdot \mathbf{a}_3 = 0 \end{cases} \Rightarrow \boldsymbol{\theta} = -\mathbf{v}_{,\alpha} \cdot \mathbf{a}_3 \mathbf{a}^\alpha \quad (9)$$

¹⁵¹ where \mathbf{a}^α 's is the in-plane contravariant base vector, $\mathbf{a}^\alpha \cdot \mathbf{a}_\beta = \delta_\beta^\alpha$, δ is the
¹⁵² Kronecker delta function. ~~Substituting~~ [The detailed derivation of Eq. 9 can be](#)
¹⁵³ [found in reference \[30\].](#)

¹⁵⁴ Furthermore, substituting Eq. (9) into Eq. (8) leads to:

$$\kappa_{\alpha\beta} = (\Gamma_{\alpha\beta}^\gamma \mathbf{v}_{,\gamma} - \mathbf{v}_{,\alpha\beta}) \cdot \mathbf{a}_3 = -\mathbf{v}_{,\alpha}|_\beta \cdot \mathbf{a}_3 \quad (10)$$

¹⁵⁵ in which $\Gamma_{\alpha\beta}^\gamma = \mathbf{a}_{\alpha,\beta} \cdot \mathbf{a}^\gamma$ is namely the Christoffel symbol of the second kind,
¹⁵⁶ and $\mathbf{v}_{,\alpha}|_\beta$ is the in-plane covariant derivative of $\mathbf{v}_{,\alpha}$, i.e. $\mathbf{v}_{,\alpha}|_\beta = \Gamma_{\alpha\beta}^\gamma \mathbf{v}_{,\gamma} - \mathbf{v}_{,\alpha\beta}$.

¹⁵⁷ 2.2. Galerkin weak form for Hu-Washizu principle of complementary energy

¹⁵⁸ In this study, the Hu-Washizu variational principle of complementary energy
¹⁵⁹ [31] was adopted for the development of the proposed analytical approach, the

¹⁶⁰ corresponding complementary functional, denoted by Π_C , is listed as follows:

$$\begin{aligned} & \Pi_C(\varepsilon_{\alpha\beta}, \kappa_{\alpha\beta}, N^{\alpha\beta}, M^{\alpha\beta}) \\ &= \int_{\Omega} \frac{h}{2} \varepsilon_{\alpha\beta} C^{\alpha\beta\gamma\eta} \varepsilon_{\gamma\eta} d\Omega + \int_{\Omega} \frac{h^3}{24} \kappa_{\alpha\beta} C^{\alpha\beta\gamma\eta} \kappa_{\gamma\eta} d\Omega \\ &+ \int_{\Omega} \varepsilon_{\alpha\beta} (N^{\alpha\beta} - h C^{\alpha\beta\gamma\eta} \varepsilon_{\gamma\eta}) d\Omega + \int_{\Omega} \kappa_{\alpha\beta} (M^{\alpha\beta} - \frac{h^3}{12} C^{\alpha\beta\gamma\eta} \kappa_{\gamma\eta}) d\Omega \\ &- \int_{\Gamma_v} \mathbf{T} \cdot \bar{\mathbf{v}} d\Gamma + \int_{\Gamma_\theta} M_{\mathbf{n}\mathbf{n}} \bar{\theta}_{\mathbf{n}} d\Gamma - (P \mathbf{a}_3 \cdot \bar{\mathbf{v}})_{\mathbf{x} \in C_w} \end{aligned} \quad (11)$$

¹⁶¹ where $C^{\alpha\beta\gamma\eta}$'s represent the components of fourth order elasticity tensor with
¹⁶² respect to the covariant base and plane stress assumption, and it can be ex-
¹⁶³ pressed by Young's modulus E , Poisson's ratio ν and the in-plane contravariant
¹⁶⁴ metric coefficients $a^{\alpha\beta}$'s, $a^{\alpha\beta} = \mathbf{a}^\alpha \cdot \mathbf{a}^\beta$, as follows:

$$C^{\alpha\beta\gamma\eta} = \frac{E}{2(1+\nu)} (a^{\alpha\gamma} a^{\beta\eta} + a^{\alpha\eta} a^{\beta\gamma} + \frac{2\nu}{1-\nu} a^{\alpha\beta} a^{\gamma\eta}) \quad (12)$$

¹⁶⁵ and $N^{\alpha\beta}$, $M^{\alpha\beta}$ are the components of membrane and bending stresses given by:

$$N^{\alpha\beta} = h C^{\alpha\beta\gamma\eta} \varepsilon_{\gamma\eta}, \quad M^{\alpha\beta} = \frac{h^3}{12} C^{\alpha\beta\gamma\eta} \kappa_{\gamma\eta} \quad (13)$$

¹⁶⁶ Essential boundaries on the edges and corners denoted by Γ_v , Γ_θ and C_v are
¹⁶⁷ naturally existed in complementary energy functional, $\bar{\mathbf{v}}$, $\bar{\theta}_{\mathbf{n}}$ are the correspond-
¹⁶⁸ ing prescribed displacement and normal rotation, respectively. \mathbf{T} , $M_{\mathbf{n}\mathbf{n}}$ and P
¹⁶⁹ can be determined by Euler-Lagrange equations of shell problem [30] as follows:

$$\mathbf{T} = \mathbf{T}_N + \mathbf{T}_M \rightarrow \begin{cases} \mathbf{T}_N = \mathbf{a}_\alpha N^{\alpha\beta} n_\beta \\ \mathbf{T}_M = (\mathbf{a}_3 M^{\alpha\beta} s_\alpha n_\beta)_{,\gamma} s^\gamma + (\mathbf{a}_3 M^{\alpha\beta})|_\beta n_\alpha \end{cases} \quad (14)$$

$$M_{\mathbf{n}\mathbf{n}} = M^{\alpha\beta} n_\alpha n_\beta \quad (15)$$

$$P = -[[M^{\alpha\beta} s_\alpha n_\beta]] \quad (16)$$

¹⁷² where $\mathbf{n} = n^\alpha \mathbf{a}_\alpha = n_\alpha \mathbf{a}^\alpha$ and $\mathbf{s} = s^\alpha \mathbf{a}_\alpha = s_\alpha \mathbf{a}^\alpha$ are the outward normal and
¹⁷³ tangent directions on boundaries. $[[f]]$ is the jump operator defined by:

$$[[f]]_{\mathbf{x}=\mathbf{x}_c} = \lim_{\epsilon \rightarrow 0^+} (f(\mathbf{x}_c + \epsilon) - f(\mathbf{x}_c - \epsilon)), \mathbf{x}_c \in \Gamma \quad (17)$$

¹⁷⁴ where f is an arbitrary function on Γ .

¹⁷⁵ Moreover, the natural boundary conditions should be applied by Lagrangian
¹⁷⁶ multiplier method with displacement \mathbf{v} regarded as multiplier. Thus, then the
¹⁷⁷ new complementary energy functional namely Π is given by:

$$\begin{aligned} & \Pi(\mathbf{v}, \varepsilon_{\alpha\beta}, \kappa_{\alpha\beta}, N^{\alpha\beta}, M^{\alpha\beta}) \\ &= \Pi_C(\varepsilon_{\alpha\beta}, \kappa_{\alpha\beta}, N^{\alpha\beta}, M^{\alpha\beta}) + \int_{\Gamma_M} \bar{\theta}_{\mathbf{n}} (M_{\mathbf{n}\mathbf{n}} - \bar{M}_{\mathbf{n}\mathbf{n}}) d\Gamma \\ &- \int_{\Gamma_T} \mathbf{v} \cdot (\mathbf{T} - \bar{\mathbf{T}}) d\Gamma - \mathbf{v} \cdot \mathbf{a}_3 (P - \bar{P})_{\mathbf{x} \in C_P} - \int_{\Omega} \mathbf{v} \cdot (\mathbf{b} - \bar{\mathbf{b}}) d\Omega \end{aligned} \quad (18)$$

¹⁷⁸ where $\bar{\mathbf{T}}$, \bar{M}_{nn} and \bar{P} are the prescribed traction, bending moment and concentrated force on edges Γ_T , Γ_M and corner C_P respectively. All the boundaries
¹⁷⁹ meet the following geometric relationships:
¹⁸⁰

$$\begin{cases} \Gamma = \Gamma_v \cup \Gamma_T \cup \Gamma_\theta \cup \Gamma_M, & C = C_v \cup C_P, \\ \Gamma_v \cap \Gamma_T = \Gamma_\theta \cap \Gamma_M = C_v \cap C_P = \emptyset \end{cases} \quad (19)$$

¹⁸¹ and $\bar{\mathbf{b}}$ stands for the prescribed body force in Ω , \mathbf{b} also can be written based on
¹⁸² Euler-Lagrange equations [30] as:

$$\mathbf{b} = \mathbf{b}_N + \mathbf{b}_M \rightarrow \begin{cases} \mathbf{b}_N = (\mathbf{a}_\alpha N^{\alpha\beta})|_\beta \\ \mathbf{b}_M = (\mathbf{a}_3 M^{\alpha\beta})|_{\alpha\beta} \end{cases} \quad (20)$$

¹⁸³ Introducing a standard variational argument to Eq. (18), $\delta\Pi = 0$, and
¹⁸⁴ considering the arbitrariness of virtual variables, $\delta\mathbf{v}$, $\delta\varepsilon_{\alpha\beta}$, $\delta\kappa_{\alpha\beta}$, $N^{\alpha\beta}$, $M^{\alpha\beta}$
¹⁸⁵ lead to the following weak form:

$$-\int_{\Omega} h\delta\varepsilon_{\alpha\beta}C^{\alpha\beta\gamma\eta}\varepsilon_{\gamma\eta}d\Omega + \int_{\Omega} \delta\varepsilon_{\alpha\beta}N^{\alpha\beta}d\Omega = 0 \quad (21a)$$

¹⁸⁶

$$-\int_{\Omega} \frac{h^3}{12}\delta\kappa_{\alpha\beta}C^{\alpha\beta\gamma\eta}\kappa_{\gamma\eta}d\Omega + \int_{\Omega} \delta\kappa_{\alpha\beta}M^{\alpha\beta}d\Omega = 0 \quad (21b)$$

¹⁸⁷

$$\begin{aligned} \int_{\Omega} \delta N^{\alpha\beta}\varepsilon_{\alpha\beta}d\Omega - \int_{\Gamma} \delta\mathbf{T}_N \cdot \mathbf{v}d\Gamma + \int_{\Omega} \delta\mathbf{b}_N \cdot \mathbf{v}d\Omega \\ + \int_{\Gamma_v} \delta\mathbf{T}_N \cdot \mathbf{v}d\Gamma = \int_{\Gamma_v} \delta\mathbf{T}_N \cdot \bar{\mathbf{v}}d\Gamma \end{aligned} \quad (21c)$$

¹⁸⁸

$$\begin{aligned} \int_{\Omega} \delta M^{\alpha\beta}\kappa_{\alpha\beta}d\Omega - \int_{\Gamma} \delta M_{nn}\theta_n d\Gamma + \int_{\Gamma} \delta\mathbf{T}_M \cdot \mathbf{v}d\Gamma + (\delta P\mathbf{a}_3 \cdot \mathbf{v})_{\mathbf{x} \in C} + \int_{\Omega} \delta\mathbf{b}_M \cdot \mathbf{v}d\Omega \\ + \int_{\Gamma_\theta} \delta M_{nn}\theta_n d\Gamma - \int_{\Gamma_v} \delta\mathbf{T}_M \cdot \mathbf{v}d\Gamma - (\delta P\mathbf{a}_3 \cdot \mathbf{v})_{\mathbf{x} \in C_v} \\ = \int_{\Gamma_\theta} \delta M_{nn}\bar{\theta}_n d\Gamma - \int_{\Gamma_v} \delta\mathbf{T}_M \cdot \bar{\mathbf{v}}d\Gamma - (\delta P\mathbf{a}_3 \cdot \bar{\mathbf{v}})_{\mathbf{x} \in C_v} \end{aligned} \quad (21d)$$

¹⁸⁹

$$\begin{aligned} \int_{\Gamma} \delta\theta_n M_{nn}d\Gamma - \int_{\Gamma} \delta\mathbf{v} \cdot \mathbf{T}d\Gamma - (\delta\mathbf{v} \cdot \mathbf{a}_3 P)_{\mathbf{x} \in C} + \int_{\Omega} \delta\mathbf{v} \cdot \mathbf{b}d\Omega \\ - \int_{\Gamma_\theta} \delta\theta_n M_{nn}d\Gamma + \int_{\Gamma_v} \delta\mathbf{v} \cdot \mathbf{T}d\Gamma + (\delta\mathbf{v} \cdot \mathbf{a}_3 P)_{\mathbf{x} \in C_v} = - \int_{\Gamma_T} \delta\mathbf{v} \cdot \bar{\mathbf{t}}d\Gamma - \int_{\Omega} \delta\mathbf{v} \cdot \bar{\mathbf{b}}d\Omega \end{aligned} \quad (21e)$$

¹⁹⁰ where the geometric relationships of Eq. (19) is used herein.

191 **3. Mixed meshfree formulation for modified Hellinger-Reissner weak
192 form**

193 *3.1. Reproducing kernel approximation for displacement*

194 This study approximates the displacement by adopting reproducing kernel
195 approximation. As shown in Fig. 2, the mid-surface of the shell Ω is discretized
196 by a set of meshfree nodes $\{\xi_I\}_{I=1}^{n_p}$ in parametric configuration, where n_p is the
197 total number of meshfree nodes. The approximated displacement namely \mathbf{v}^h
198 can be expressed as:

$$\mathbf{v}(\xi) = \sum_{I=1}^{n_p} \Psi_I(\xi) \mathbf{d}_I \quad (22)$$

199 in which Ψ_I and \mathbf{d}_I is the shape function and nodal coefficient tensor related by
200 node ξ_I . According to reproducing kernel approximation [4], the shape function
201 takes the following form:

$$\Psi_I(\xi) = \mathbf{p}^T(\xi) \mathbf{c}(\xi) \phi(\xi_I - \xi) \quad (23)$$

202 where \mathbf{p} is the basis function vector represented using the following quadratic
203 function as:

$$\mathbf{p} = \{1, \xi^1, \xi^2, (\xi^1)^2, \xi^1 \xi^2, (\xi^2)^2\}^T \quad (24)$$

204 The kernel function denoted by ϕ controls the support and smoothness of
205 meshfree shape functions. The quintic B-spline function with square support is
206 used herein as the kernel function:

$$\phi(\xi_I - \xi) = \phi(\hat{s}_1)\phi(\hat{s}_2), \quad \hat{s}_\alpha = \frac{|\xi_I^\alpha - \xi^\alpha|}{s_{\alpha I}} \quad (25)$$

207 with

$$\phi(\hat{s}_\alpha) = \frac{1}{5!} \begin{cases} (3 - 3\hat{s}_\alpha)^5 - 6(2 - 3\hat{s}_\alpha)^5 + 15(1 - 3\hat{s}_\alpha)^5 & \hat{s}_\alpha \leq \frac{1}{3} \\ (3 - 3\hat{s}_\alpha)^5 - 6(2 - 3\hat{s}_\alpha)^5 & \frac{1}{3} < \hat{s}_\alpha \leq \frac{2}{3} \\ (3 - 3\hat{s}_\alpha)^5 & \frac{2}{3} < \hat{s}_\alpha \leq 1 \\ 0 & \hat{s}_\alpha > 1 \end{cases} \quad (26)$$

208 and $\hat{s}_{\alpha I}$ means the characterized size of support for $s_{\alpha I}$ means the support size
209 of meshfree shape function Ψ_I .

210 The unknown vector \mathbf{c} in shape function are determined by the fulfillment
211 of the so-called consistency condition:

$$\sum_{I=1}^{n_p} \Psi_I(\xi) \mathbf{p}(\xi_I) = \mathbf{p}(\xi) \quad (27)$$

212 or equivalently

$$\sum_{I=1}^{n_p} \Psi_I(\xi) \mathbf{p}(\xi_I - \xi) = \mathbf{p}(\mathbf{0}) \quad (28)$$

²¹³ Substituting Eq. (22) into (28), yields:

$$\mathbf{A}(\boldsymbol{\xi})\mathbf{c}(\boldsymbol{\xi}) = \mathbf{p}(\mathbf{0}) \Rightarrow \mathbf{c}(\boldsymbol{\xi}) = \mathbf{A}^{-1}(\boldsymbol{\xi})\mathbf{p}(\mathbf{0}) \quad (29)$$

²¹⁴ where \mathbf{A} is the moment matrix:

$$\mathbf{A}(\boldsymbol{\xi}) = \sum_{I=1}^{n_p} \phi(\boldsymbol{\xi}_I - \boldsymbol{\xi}) \mathbf{p}(\boldsymbol{\xi}_I - \boldsymbol{\xi}) \mathbf{p}^T(\boldsymbol{\xi}_I - \boldsymbol{\xi}) \quad (30)$$

²¹⁵ Substituting Eq. (29) back into Eq. (22), the expression of meshfree shape
²¹⁶ function can be written as:

$$\Psi_I(\boldsymbol{\xi}) = \mathbf{p}^T(\boldsymbol{\xi}_I - \boldsymbol{\xi}) \mathbf{A}^{-1}(\boldsymbol{\xi}) \mathbf{p}(\mathbf{0}) \phi(\boldsymbol{\xi}_I - \boldsymbol{\xi}) \quad (31)$$

²¹⁷ *3.2. Reproducing kernel gradient smoothing approximation for effective stress
²¹⁸ and strain*

²¹⁹ In Galerkin meshfree formulation, the mid-plane of thin shell Ω is split by
²²⁰ a set of integration cells Ω_C 's, $\cup_{C=1}^{n_e} \Omega_C \approx \Omega$, as shown in Fig. 2. With the
²²¹ inspiration of reproducing kernel smoothing framework, the Cartesian and co-
²²² variant derivatives of displacement, $\mathbf{v}_{,\alpha}$ and $-\mathbf{v}_{,\alpha}|_\beta$, in strains $\varepsilon_{\alpha\beta}$, $\kappa_{\alpha\beta}$ are
²²³ approximated by $(p-1)$ -th order polynomials in each integration cells. In inte-
²²⁴ gration cell Ω_C , the approximated derivatives and strains denoted by $\mathbf{v}_{,\alpha}^h$, $\varepsilon_{\alpha\beta}^h$
²²⁵ and $-\mathbf{v}_{,\alpha}|_\beta$, $\kappa_{\alpha\beta}^h$ can be expressed by:

$$\mathbf{v}_{,\alpha}^h(\boldsymbol{\xi}) = \mathbf{q}^T(\boldsymbol{\xi}) \mathbf{d}_\alpha^\varepsilon, \quad \varepsilon_{\alpha\beta}^h(\boldsymbol{\xi}) = \mathbf{q}^T(\boldsymbol{\xi}) \frac{1}{2} (\mathbf{a}_\alpha \cdot \mathbf{d}_\beta^\varepsilon + \mathbf{a}_\beta \cdot \mathbf{d}_\alpha^\varepsilon) \quad (32)$$

$$-\mathbf{v}_{,\alpha}|_\beta(\boldsymbol{\xi}) = \mathbf{q}^T(\boldsymbol{\xi}) \mathbf{d}_{\alpha\beta}^\kappa, \quad \kappa_{\alpha\beta}^h(\boldsymbol{\xi}) = \mathbf{q}^T(\boldsymbol{\xi}) \mathbf{a}_3 \cdot \mathbf{d}_{\alpha\beta}^\kappa \quad (33)$$

²²⁶ where \mathbf{q} is the linear polynomial vector and has the following form:

$$\mathbf{q} = \{1, \xi^1, \xi^2\}^T \quad (34)$$

²²⁸ and the $\mathbf{d}_\alpha^\varepsilon$, $\mathbf{d}_{\alpha\beta}^\kappa$ are the corresponding coefficient vector tensors. For the con-
²²⁹ ciseness, the mixed usage of tensor and vector is introduced in this study. For
²³⁰ instance, the component of coefficient tensor vector $\mathbf{d}_{\alpha I}^\varepsilon$, $\mathbf{d}_\alpha^\varepsilon = \{\mathbf{d}_{\alpha I}^\varepsilon\}$, is a three
²³¹ dimensional tensor, $\dim \mathbf{d}_{\alpha I}^\varepsilon = \dim \mathbf{v}$.

²³² In order to meet the integration constraint of thin shell problem, the ap-
²³³ proximated stresses $N^{\alpha\beta h}$, $M^{\alpha\beta h}$ are assumed to be a similar form with strains,
²³⁴ yields:

$$N^{\alpha\beta h}(\boldsymbol{\xi}) = \mathbf{q}^T(\boldsymbol{\xi}) \mathbf{a}^\alpha \cdot \mathbf{d}_N^\beta, \quad \mathbf{a}_\alpha N^{\alpha\beta h}(\boldsymbol{\xi}) = \mathbf{q}^T(\boldsymbol{\xi}) \mathbf{d}_N^\beta \quad (35)$$

$$M^{\alpha\beta h}(\boldsymbol{\xi}) = \mathbf{q}^T(\boldsymbol{\xi}) \mathbf{a}_3 \cdot \mathbf{d}_M^{\alpha\beta}, \quad \mathbf{a}_3 M^{\alpha\beta h}(\boldsymbol{\xi}) = \mathbf{q}^T(\boldsymbol{\xi}) \mathbf{d}_M^{\alpha\beta} \quad (36)$$

²³⁵ substituting the approximations of Eqs. (22), (32), (33), (35), (36) into Eqs.
²³⁶ (21c), (21d) can express $\mathbf{d}_\beta^\varepsilon$ and $\mathbf{d}_{\alpha\beta}^\kappa$ by \mathbf{d} as:

$$\mathbf{d}_\beta^\varepsilon = \mathbf{G}^{-1} \left(\sum_{I=1}^{n_p} (\tilde{\mathbf{g}}_{\beta I} - \bar{\mathbf{g}}_{\beta I}) \mathbf{d}_I + \hat{\mathbf{g}}_\beta \right) \quad (37)$$

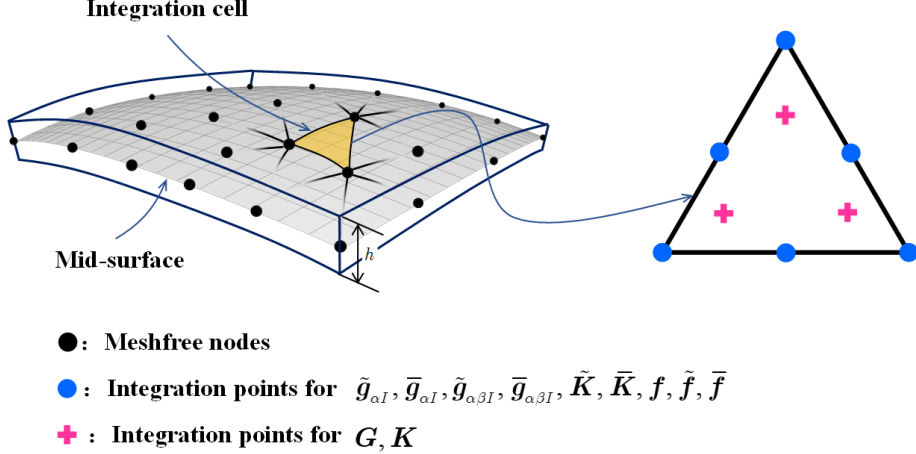


Figure 2: Integration scheme for Hu-Washizu weak form.

238

$$\mathbf{d}_{\alpha\beta}^\kappa = \mathbf{G}^{-1} \left(\sum_{I=1}^{n_p} (\tilde{\mathbf{g}}_{\alpha\beta I} - \bar{\mathbf{g}}_{\alpha\beta I}) \mathbf{d}_I + \hat{\mathbf{g}}_{\alpha\beta} \right) \quad (38)$$

239 with

$$\mathbf{G} = \int_{\Omega_C} \mathbf{q}^T \mathbf{q} d\Omega \quad (39)$$

240

$$\tilde{\mathbf{g}}_{\beta I} = \int_{\Gamma_C} \Psi_I \mathbf{q} n_\beta d\Gamma - \int_{\Omega_C} \Psi_I \mathbf{q}_{|\beta} d\Omega \quad (40a)$$

$$\bar{\mathbf{g}}_{\beta I} = \int_{\Gamma_C \cap \Gamma_v} \Psi_I \mathbf{q} n_\beta d\Gamma \quad (40b)$$

$$\hat{\mathbf{g}}_\beta = \int_{\Gamma_C \cap \Gamma_v} \mathbf{q} n_\beta \bar{\mathbf{v}} d\Gamma \quad (40c)$$

241

$$\begin{aligned} \tilde{\mathbf{g}}_{\alpha\beta I} &= \int_{\Gamma_C} \Psi_{I,\gamma} n^\gamma \mathbf{q} n_\alpha n_\beta d\Gamma - \int_{\Gamma_C} \Psi_I (\mathbf{q}_{|\beta} n_\alpha + (\mathbf{q} s_\alpha n_\beta)_{,\gamma} s^\gamma) d\Gamma \\ &\quad + [[\Psi_I \mathbf{q} s_\alpha n_\beta]]_{\mathbf{x} \in C_C} - \int_{\Omega_C} \Psi_I \mathbf{q}_{,\alpha|\beta} d\Omega \end{aligned} \quad (41a)$$

$$\begin{aligned} \bar{\mathbf{g}}_{\alpha\beta I} &= \int_{\Gamma_C \cap \Gamma_\theta} \Psi_{I,\gamma} n^\gamma \mathbf{q} n_\alpha n_\beta d\Gamma - \int_{\Gamma_C \cap \Gamma_v} \Psi_I (\mathbf{q}_{|\beta} n_\alpha + (\mathbf{q} s_\alpha n_\beta)_{,\gamma} s^\gamma) d\Gamma \\ &\quad + [[\Psi_I \mathbf{q} s_\alpha n_\beta]]_{\mathbf{x} \in C_C \cap C_v} \end{aligned} \quad (41b)$$

$$\begin{aligned} \hat{\mathbf{g}}_{\alpha\beta} &= \int_{\Gamma_C \cap \Gamma_\theta} \mathbf{q} n_\alpha n_\beta \bar{\mathbf{a}}_3 \bar{\mathbf{n}} d\Gamma - \int_{\Gamma_C \cap \Gamma_v} (\mathbf{q}_{|\beta} n_\alpha + (\mathbf{q} s_\alpha n_\beta)_{,\gamma} s^\gamma) \bar{\mathbf{v}} d\Gamma \\ &\quad + [[\mathbf{q} s_\alpha n_\beta \bar{\mathbf{v}}]]_{\mathbf{x} \in C_C \cap C_v} \end{aligned} \quad (41c)$$

²⁴² where evaluations of $\mathbf{q}_{|\beta}$, $\mathbf{q}_{,\alpha|\beta}$ are detail in Appendix A. Further plugging Eqs.
²⁴³ (37) and (38) back into Eqs. (32) and (33) respectively gives the final expression
²⁴⁴ of $\mathbf{v}_{,\alpha}^h$, $\varepsilon_{\alpha\beta}^h$ and $-\mathbf{v}_{,\alpha\beta}^h$, $\kappa_{\alpha\beta}^h$ as:

$$\mathbf{v}_{,\alpha}^h = \sum_{I=1}^{n_p} (\tilde{\Psi}_{I,\alpha} - \bar{\Psi}_{I,\alpha}) \mathbf{d}_I + \mathbf{q}^T \mathbf{G}^{-1} \hat{\mathbf{g}}_\alpha \quad (42a)$$

$$\begin{aligned} \varepsilon_{\alpha\beta}^h &= \sum_{I=1}^{n_p} \frac{1}{2} (\mathbf{a}_\alpha \tilde{\Psi}_{I,\beta} + \mathbf{a}_\beta \tilde{\Psi}_{I,\alpha}) \cdot \mathbf{d}_I - \sum_{I=1}^{n_p} \frac{1}{2} (\mathbf{a}_\alpha \bar{\Psi}_{I,\beta} + \mathbf{a}_\beta \bar{\Psi}_{I,\alpha}) \cdot \mathbf{d}_I \\ &\quad + \mathbf{q}^T \mathbf{G}^{-1} \frac{1}{2} (\mathbf{a}_\alpha \cdot \hat{\mathbf{g}}_\beta + \mathbf{a}_\beta \cdot \hat{\mathbf{g}}_\alpha) \\ &= \tilde{\varepsilon}_{\alpha\beta}^h - \bar{\varepsilon}_{\alpha\beta}^h + \hat{\varepsilon}_{\alpha\beta}^h \end{aligned} \quad (42b)$$

$$-\mathbf{v}_{,\alpha}^h|_\beta = \sum_{I=1}^{n_p} (\tilde{\Psi}_{I,\alpha\beta} - \bar{\Psi}_{I,\alpha\beta}) \mathbf{d}_I + \mathbf{q}^T \mathbf{G}^{-1} \hat{\mathbf{g}}_{\alpha\beta} \quad (43a)$$

$$\begin{aligned} \kappa_{\alpha\beta}^h &= \sum_{I=1}^{n_p} \tilde{\Psi}_{I,\alpha\beta} \mathbf{a}_3 \cdot \mathbf{d}_I - \sum_{I=1}^{n_p} \bar{\Psi}_{I,\alpha\beta} \mathbf{a}_3 \cdot \mathbf{d}_I + \mathbf{q}^T \mathbf{G}^{-1} \mathbf{a}_3 \cdot \hat{\mathbf{g}}_{\alpha\beta} \\ &= \tilde{\kappa}_{\alpha\beta}^h - \bar{\kappa}_{\alpha\beta}^h + \hat{\kappa}_{\alpha\beta}^h \end{aligned} \quad (43b)$$

²⁴⁸ with

$$\begin{cases} \tilde{\varepsilon}_{\alpha\beta}^h = \sum_{I=1}^{n_p} \frac{1}{2} (\mathbf{a}_\alpha \tilde{\Psi}_{I,\beta} + \mathbf{a}_\beta \tilde{\Psi}_{I,\alpha}) \cdot \mathbf{d}_I = \sum_{I=1}^{n_p} \tilde{\varepsilon}_{\alpha\beta I} \cdot \mathbf{d}_I \\ \bar{\varepsilon}_{\alpha\beta}^h = \sum_{I=1}^{n_p} \frac{1}{2} (\mathbf{a}_\alpha \bar{\Psi}_{I,\beta} + \mathbf{a}_\beta \bar{\Psi}_{I,\alpha}) \cdot \mathbf{d}_I = \sum_{I=1}^{n_p} \bar{\varepsilon}_{\alpha\beta I} \cdot \mathbf{d}_I \\ \hat{\varepsilon}_{\alpha\beta}^h = \mathbf{q}^T \mathbf{G}^{-1} \frac{1}{2} (\mathbf{a}_\alpha \cdot \hat{\mathbf{g}}_\beta + \mathbf{a}_\beta \cdot \hat{\mathbf{g}}_\alpha) \end{cases} \quad (44)$$

$$\begin{cases} \tilde{\Psi}_{I,\alpha}(\boldsymbol{\xi}) = \mathbf{q}^T(\boldsymbol{\xi}) \mathbf{G}^{-1} \tilde{\mathbf{g}}_{\alpha I} \\ \bar{\Psi}_{I,\alpha}(\boldsymbol{\xi}) = \mathbf{q}^T(\boldsymbol{\xi}) \mathbf{G}^{-1} \bar{\mathbf{g}}_{\alpha I} \\ \tilde{\varepsilon}_{\alpha\beta I} = \frac{1}{2} (\mathbf{a}_\alpha \tilde{\Psi}_{I,\beta} + \mathbf{a}_\beta \tilde{\Psi}_{I,\alpha}) \\ \bar{\varepsilon}_{\alpha\beta I} = \frac{1}{2} (\mathbf{a}_\alpha \bar{\Psi}_{I,\beta} + \mathbf{a}_\beta \bar{\Psi}_{I,\alpha}) \end{cases} \quad (45)$$

$$\begin{cases} \tilde{\kappa}_{\alpha\beta}^h = \sum_{I=1}^{n_p} \tilde{\Psi}_{I,\alpha\beta} \mathbf{a}_3 \cdot \mathbf{d}_I = \sum_{I=1}^{n_p} \tilde{\kappa}_{\alpha\beta I} \cdot \mathbf{d}_I \\ \bar{\kappa}_{\alpha\beta}^h = \sum_{I=1}^{n_p} \bar{\Psi}_{I,\alpha\beta} \mathbf{a}_3 \cdot \mathbf{d}_I = \sum_{I=1}^{n_p} \bar{\kappa}_{\alpha\beta I} \cdot \mathbf{d}_I \\ \hat{\kappa}_{\alpha\beta}^h = \mathbf{q}^T \mathbf{G}^{-1} \mathbf{a}_3 \cdot \hat{\mathbf{g}}_{\alpha\beta} \end{cases} \quad (46)$$

251

$$\begin{cases} \tilde{\Psi}_{I,\alpha\beta}(\xi) = \mathbf{q}^T(\xi) \mathbf{G}^{-1} \tilde{\mathbf{g}}_{\alpha\beta I} \\ \bar{\Psi}_{I,\alpha\beta}(\xi) = \mathbf{q}^T(\xi) \mathbf{G}^{-1} \tilde{\mathbf{g}}_{\alpha\beta I} \\ \tilde{\kappa}_{\alpha\beta I} = \tilde{\Psi}_{I,\alpha\beta} \mathbf{a}_3 \\ \bar{\kappa}_{\alpha\beta I} = \bar{\Psi}_{I,\alpha\beta} \mathbf{a}_3 \end{cases} \quad (47)$$

252 It has to be noted that, referring to reproducing kernel gradient smoothing
 253 framework [26], $\tilde{\Psi}_{I,\alpha}$, $\tilde{\Psi}_{I,\alpha\beta}$ are actually the first and second order smoothed
 254 gradients in curvilinear coordinates. $\tilde{\mathbf{g}}_{\alpha I}$ and $\tilde{\mathbf{g}}_{\alpha\beta I}$ are the right hand side inte-
 255 gration constraints for first and second order gradients, then this formulation can
 256 meet the variational consistency for the ~~p -th second~~ order polynomials. It should
 257 be known that, in curved model, the variational consistency for non-polynomial
 258 functions, like trigonometric functions, should be required for the polynomial
 259 solution. Even with ~~p -th order high order polynomial~~ variational consistency,
 260 the proposed formulation can not exactly reproduce the solution spanned by
 261 basis functions. However, the accuracy of reproducing kernel smoothed gradi-
 262 ents is still better than traditional meshfree formulation. Numerical examples
 263 in the section below will provide better evidence to prove the accuracy of the
 264 reproducing kernel smoothed gradients.

265 **4. Naturally variational enforcement for essential boundary condi-**
 266 **tions**

267 *4.1. Discrete equilibrium equations*

268 With the approximated effective stresses and strains, the last equation of
 269 weak form Eq. (21e) becomes:

$$-\sum_{C=1}^{n_e} \sum_{I=1}^{n_p} \delta \mathbf{d}_I \cdot \left((\tilde{\mathbf{g}}_{\alpha I}^T - \bar{\mathbf{g}}_{\alpha I}^T) \mathbf{d}_N^\alpha + (\tilde{\mathbf{g}}_{\alpha\beta I}^T - \bar{\mathbf{g}}_{\alpha\beta I}^T) \mathbf{d}_M^{\alpha\beta} \right) = -\sum_{I=1}^{n_p} \delta d_I \cdot \mathbf{f}_I \quad (48)$$

270 where \mathbf{f}_I 's are the components of the traditional force vector:

$$\mathbf{f}_I = \int_{\Gamma_t} \Psi_I \bar{\mathbf{t}} d\Gamma - \int_{\Gamma_M} \Psi_{I,\gamma} n^\gamma \bar{M}_{\mathbf{n}\mathbf{n}} d\Gamma + [[\Psi_I \mathbf{a}_3 \bar{P}]]_{\mathbf{x} \in C_P} + \int_{\Omega} \Psi_I \bar{\mathbf{b}} d\Omega \quad (49)$$

271 The left side of Eq. (48) can be simplified using the following steps. For clarity,
 272 the derivation of first term in Eq. (48) taken as an example is given by:

$$\begin{aligned} \sum_{I=1}^{n_p} \delta \mathbf{d}_I \cdot \tilde{\mathbf{g}}_{\alpha I}^T \mathbf{d}_N^\alpha &= \sum_{I=1}^{n_p} \delta \mathbf{d}_I \cdot (\mathbf{G}^{-1} \tilde{\mathbf{g}}_{\alpha I})^T \mathbf{G} \mathbf{d}_N^\alpha \\ &= \int_{\Omega_C} \sum_{I=1}^{n_p} \delta \mathbf{d}_I \cdot (\mathbf{q}^T \mathbf{G}^{-1} \tilde{\mathbf{g}}_{\alpha I})^T \mathbf{q}^T \mathbf{d}_N^\alpha d\Omega \\ &= \int_{\Omega_C} \sum_{I=1}^{n_p} \delta \mathbf{d}_I \cdot \mathbf{a}_\beta (\mathbf{q}^T \mathbf{G}^{-1} \tilde{\mathbf{g}}_{\alpha I})^T N^{\alpha\beta h} d\Omega \\ &= \int_{\Omega_C} \delta \hat{\varepsilon}_{\alpha\beta}^h N^{\alpha\beta h} d\Omega \end{aligned} \quad (50)$$

²⁷³ following the above procedure and including the weak form of Eqs. (21a), (21b),
²⁷⁴ the left side of Eq. (48) in Ω_C becomes:

$$\begin{aligned}
& \sum_{I=1}^{n_p} \delta \mathbf{d}_I \cdot \left((\tilde{\mathbf{g}}_{\alpha I}^T - \bar{\mathbf{g}}_{\alpha I}^T) \mathbf{d}_N^\alpha + (\tilde{\mathbf{g}}_{\alpha \beta I}^T - \bar{\mathbf{g}}_{\alpha \beta I}^T) \mathbf{d}_M^{\alpha \beta} \right) \\
& = \int_{\Omega_C} ((\delta \tilde{\varepsilon}_{\alpha \beta}^h - \delta \bar{\varepsilon}_{\alpha \beta}^h) N^{\alpha \beta h} + (\delta \tilde{\kappa}_{\alpha \beta}^h - \delta \bar{\kappa}_{\alpha \beta}^h) M^{\alpha \beta h}) d\Omega \\
& = \int_{\Omega_C} (\delta \tilde{\varepsilon}_{\alpha \beta}^h - \delta \bar{\varepsilon}_{\alpha \beta}^h) h C^{\alpha \beta \gamma \eta} \varepsilon_{\gamma \eta}^h + (\delta \tilde{\kappa}_{\alpha \beta}^h - \delta \bar{\kappa}_{\alpha \beta}^h) \frac{h^3}{12} C^{\alpha \beta \gamma \eta} \kappa_{\gamma \eta}^h \\
& = \int_{\Omega_C} \delta \tilde{\varepsilon}_{\alpha \beta}^h h C^{\alpha \beta \gamma \eta} \tilde{\varepsilon}_{\gamma \eta}^h d\Omega + \int_{\Omega_C} \delta \tilde{\kappa}_{\alpha \beta}^h \frac{h^3}{12} C^{\alpha \beta \gamma \eta} \tilde{\kappa}_{\gamma \eta}^h d\Omega \\
& - \int_{\Omega_C} \delta \tilde{\varepsilon}_{\alpha \beta}^h h C^{\alpha \beta \gamma \eta} \bar{\varepsilon}_{\gamma \eta}^h d\Omega - \int_{\Omega_C} \delta \tilde{\varepsilon}_{\alpha \beta}^h h C^{\alpha \beta \gamma \eta} \hat{\varepsilon}_{\gamma \eta}^h d\Omega \\
& - \int_{\Omega_C} \delta \tilde{\kappa}_{\alpha \beta}^h \frac{h^3}{12} C^{\alpha \beta \gamma \eta} \bar{\kappa}_{\gamma \eta}^h d\Omega - \int_{\Omega_C} \delta \tilde{\kappa}_{\alpha \beta}^h \frac{h^3}{12} C^{\alpha \beta \gamma \eta} \hat{\kappa}_{\gamma \eta}^h d\Omega \\
& + \int_{\Omega_C} \delta \bar{\varepsilon}_{\alpha \beta}^h h C^{\alpha \beta \gamma \eta} \tilde{\varepsilon}_{\gamma \eta}^h d\Omega + \int_{\Omega_C} \delta \bar{\kappa}_{\alpha \beta}^h \frac{h^3}{12} C^{\alpha \beta \gamma \eta} \tilde{\kappa}_{\gamma \eta}^h d\Omega \\
& + \int_{\Omega_C} (\delta \tilde{\varepsilon}_{\alpha \beta}^h - \delta \bar{\varepsilon}_{\alpha \beta}^h) h C^{\alpha \beta \gamma \eta} \hat{\varepsilon}_{\gamma \eta}^h d\Omega + \int_{\Omega_C} (\delta \tilde{\kappa}_{\alpha \beta}^h - \delta \bar{\kappa}_{\alpha \beta}^h) \frac{h^3}{12} C^{\alpha \beta \gamma \eta} \hat{\kappa}_{\gamma \eta}^h d\Omega
\end{aligned} \tag{51}$$

²⁷⁵ on further substituting Eqs. (44) and (46) into above equation gives the final
²⁷⁶ discrete equilibrium equations, respectively:

$$(\mathbf{K} + \tilde{\mathbf{K}} + \bar{\mathbf{K}}) \mathbf{d} = \mathbf{f} + \tilde{\mathbf{f}} + \bar{\mathbf{f}} \tag{52}$$

²⁷⁷ where

$$\mathbf{K}_{IJ} = \int_{\Omega} \tilde{\varepsilon}_{\alpha \beta I} h C^{\alpha \beta \gamma \eta} \tilde{\varepsilon}_{\gamma \eta J} d\Omega + \int_{\Omega} \tilde{\kappa}_{\alpha \beta I} \frac{h^3}{12} C^{\alpha \beta \gamma \eta} \tilde{\kappa}_{\alpha \beta J} d\Omega \tag{53}$$

²⁷⁸

$$\begin{aligned}
\tilde{\mathbf{K}}_{IJ} = & - \int_{\Gamma_v} (\Psi_I \tilde{\mathbf{T}}_{NJ} + \tilde{\mathbf{T}}_{NJ} \Psi_J) d\Gamma \\
& + \int_{\Gamma_\theta} (\Psi_{I,\gamma} n^\gamma \mathbf{a}_3 \tilde{\mathbf{M}}_{nnJ} + \mathbf{a}_3 \tilde{\mathbf{M}}_{nnI} \Psi_{I,\gamma} n^\gamma) d\Gamma \\
& + ([[\Psi_I \mathbf{a}_3 \tilde{\mathbf{P}}_J]] + [[\tilde{\mathbf{P}}_I \mathbf{a}_3 \Psi_J]])_{\mathbf{x} \in C_v}
\end{aligned} \tag{54a}$$

$$\tilde{\mathbf{f}}_I = - \int_{\Gamma_v} \tilde{\mathbf{T}}_{NI} \cdot \bar{\mathbf{v}} d\Gamma + \int_{\Gamma_\theta} \tilde{\mathbf{M}}_{nnI} \bar{\theta}_n d\Gamma + [[\tilde{\mathbf{P}}_I \mathbf{a}_3 \cdot \bar{\mathbf{v}}]]_{\mathbf{x} \in C_v} \tag{54b}$$

²⁷⁹

$$\bar{\mathbf{K}}_{IJ} = - \int_{\Gamma_v} \bar{\mathbf{T}}_{MI} \Psi_J d\Gamma + \int_{\Gamma_\theta} \mathbf{a}_3 \bar{\mathbf{M}}_{nnI} \Psi_{J,\gamma} n^\gamma d\Gamma + [[\bar{\mathbf{P}}_I \mathbf{a}_3 \Psi_J]]_{\mathbf{x} \in C_v} \tag{55a}$$

$$\bar{\mathbf{f}}_I = - \int_{\Gamma_v} \bar{\mathbf{T}}_{MI} \cdot \bar{\mathbf{v}} d\Gamma + \int_{\Gamma_\theta} \bar{\mathbf{M}}_{nnI} \bar{\theta}_n d\Gamma + [[\bar{\mathbf{P}}_I \mathbf{a}_3 \cdot \bar{\mathbf{v}}]]_{\mathbf{x} \in C_v} \tag{55b}$$

280 The detailed derivations of Eqs (53)-(55) are listed in the Appendix B.
 281 As shown in these equations, Eq. (53) is the conventional stiffness matrix
 282 evaluated by smoothed gradients $\tilde{\Psi}_{I,\alpha}$, $\tilde{\Psi}_{I,\alpha}|_{\beta}$, and the Eqs. (54) and (55)
 283 contribute for the enforcement of essential boundary. It should be mentioned
 284 that, in accordance with reproducing kernel smoothed gradient framework, the
 285 integration scheme of Eqs. (53-55) should be aligned with the those used in
 286 the construction of smoothed gradients. The integration scheme used for pro-
 287 posed method is shown in Fig. 2, ~~the in which the total number of the blue~~
 288 ~~circular integration points has been optimized from a global point of view,~~
 289 ~~aiming to reduce the computation of traditional meshfree shape functions and~~
 290 ~~its first order derivatives. In contrast, for assembly stiffness matrix K , the~~
 291 ~~low order Gauss integration rule is suitable to ensure the accuracy due to the~~
 292 ~~inherently variational consistency in smoothed gradients. The detailed pos-~~
 293 ~~tions and weight of integration points and the efficiency demonstration of this~~
 294 ~~optimized integration scheme~~ can be found in [32]-[26, 32]. With a close look
 295 at Eqs. (54) and (55), the proposed approach for enforcing essential boundary
 296 conditions show an identical structure with traditional Nitsche's method, both
 297 have the consistent and stabilized terms. So, the next subsection will review
 298 the Nitsche's method and compare it with the proposed method.

299 *4.2. Comparison with Nitsche's method*

300 The Nitsche's method for enforcing essential boundaries can be regarded as a
 301 combination of Lagrangian multiplier method and penalty method, in which the
 302 Lagrangian multiplier is represented by the approximated displacement. The
 303 corresponding total potential energy functional Π_P is given by:

$$\begin{aligned}
 \underline{\Pi_P(\mathbf{v})} = & \int_{\Omega} \frac{1}{2} \varepsilon_{\alpha\beta} N^{\alpha\beta} d\Omega + \int_{\Omega} \frac{1}{2} \kappa_{\alpha\beta} M^{\alpha\beta} d\Omega \\
 & - \int_{\Gamma_t} \mathbf{v} \cdot \bar{\mathbf{t}} d\Gamma + \int_{\Gamma_M} \mathbf{v}_{,\gamma} n^\gamma \mathbf{a}_3 M_{nn} d\Gamma + (\mathbf{v} \cdot \mathbf{a}_3 P)_{\mathbf{x} \in C_P} - \int_{\Omega} \mathbf{v} \cdot \bar{\mathbf{b}} d\Omega \\
 & - \underbrace{\int_{\Gamma_v} \mathbf{t} \cdot (\mathbf{v} - \bar{\mathbf{v}}) d\Gamma + \int_{\Gamma_\theta} M_{nn} (\theta_{\mathbf{n}} - \bar{\theta}_{\mathbf{n}}) d\Gamma + (P \mathbf{a}_3 \cdot (\mathbf{v} - \bar{\mathbf{v}}))_{\mathbf{x} \in C_v}}_{\text{consistent term}} \\
 & + \underbrace{\frac{\alpha_v}{2} \int_{\Gamma_v} \mathbf{v} \cdot \mathbf{v} d\Gamma + \frac{\alpha_\theta}{2} \int_{\Gamma_\theta} \theta_{\mathbf{n}}^2 d\Gamma + \frac{\alpha_C}{2} (\mathbf{v} \cdot \mathbf{v})_{\mathbf{x} \in C_v}}_{\text{stabilized term}}
 \end{aligned}$$

304

$$\begin{aligned}
\Pi_P(\mathbf{v}) = & \underbrace{\int_{\Omega} \frac{1}{2} \varepsilon_{\alpha\beta} N^{\alpha\beta} d\Omega + \int_{\Omega} \frac{1}{2} \kappa_{\alpha\beta} M^{\alpha\beta} d\Omega}_{-\int_{\Gamma_t} \mathbf{v} \cdot \bar{\mathbf{t}} d\Gamma + \int_{\Gamma_M} \mathbf{v}_{,\gamma} n^\gamma \mathbf{a}_3 M_{nn} d\Gamma + (\mathbf{v} \cdot \mathbf{a}_3 P)_{x \in C_P} - \int_{\Omega} \mathbf{v} \cdot \bar{\mathbf{b}} d\Omega} \\
& - \underbrace{\int_{\Gamma_v} \mathbf{t} \cdot (\mathbf{v} - \bar{\mathbf{v}}) d\Gamma + \int_{\Gamma_\theta} M_{nn} (\theta_n - \bar{\theta}_n) d\Gamma + (P \mathbf{a}_3 \cdot (\mathbf{v} - \bar{\mathbf{v}}))_{x \in C_v}}_{\text{consistent term}} \\
& + \underbrace{\sum_{i=1}^3 \frac{\alpha_{vi}}{2} \int_{\Gamma_v} \mathbf{v} \cdot \mathbf{v} d\Gamma + \frac{\alpha_\theta}{2} \int_{\Gamma_\theta} \theta_n^2 d\Gamma + \frac{\alpha_C}{2} (\mathbf{v} \cdot \mathbf{a}_3)_{x \in C_v}^2}_{\text{stabilized term}} \quad (56)
\end{aligned}$$

305 where the consistent term generated from the Lagrangian multiplier method
306 contributes to enforce the essential boundary, and meet the variational consistency condition.
307 However, the consistent term can not always ensure the coercivity of stiffness, so the penalty method is introduced to serve as a stabilized term, in which α_{vi} 's, α_θ and α_C are experimental artificial parameters in penalty method. With a standard variational argument, the corresponding
309 weak form can be stated as:
310

$$\begin{aligned}
\delta\Pi_P(\mathbf{v}) = & \underbrace{\int_{\Omega} \delta\varepsilon_{\alpha\beta} N^{\alpha\beta} d\Omega + \int_{\Omega} \delta\kappa_{\alpha\beta} M^{\alpha\beta} d\Omega}_{-\int_{\Gamma_t} \delta\mathbf{v} \cdot \bar{\mathbf{t}} d\Gamma + \int_{\Gamma_M} \delta\mathbf{v}_{,\gamma} n^\gamma \mathbf{a}_3 M_{nn} d\Gamma + (\delta\mathbf{v} \cdot \mathbf{a}_3 P)_{x \in C_P} - \int_{\Omega} \delta\mathbf{v} \cdot \bar{\mathbf{b}} d\Omega} \\
& - \underbrace{\int_{\Gamma_v} \delta\mathbf{v} \cdot \mathbf{t} d\Gamma + \int_{\Gamma_\theta} \delta\theta_n M_{nn} d\Gamma + (\mathbf{v} \cdot \mathbf{a}_3 P)_{x \in C_v}}_{-\int_{\Gamma_v} \delta\mathbf{t} \cdot (\mathbf{v} - \bar{\mathbf{v}}) d\Gamma + \int_{\Gamma_\theta} \delta M_{nn} (\theta_n - \bar{\theta}_n) d\Gamma + (\delta P \mathbf{a}_3 \cdot (\mathbf{v} - \bar{\mathbf{v}}))_{x \in C_v}} \\
& + \underbrace{\alpha_v \int_{\Gamma_v} \delta\mathbf{v} \cdot \mathbf{v} d\Gamma + \alpha_\theta \int_{\Gamma_\theta} \delta\theta_n \theta_n d\Gamma + \alpha_C (\delta\mathbf{v} \cdot \mathbf{v})_{x \in C_v}}_{+ \alpha_v \int_{\Gamma_v} \delta\mathbf{v} \cdot \mathbf{v} d\Gamma + \alpha_\theta \int_{\Gamma_\theta} \delta\theta_n \theta_n d\Gamma + \alpha_C (\delta\mathbf{v} \cdot \mathbf{v})_{x \in C_v}} \\
& = 0
\end{aligned}$$

312

$$\begin{aligned}
& \delta\Pi_P(\mathbf{v}) = \int_{\Omega} \delta\varepsilon_{\alpha\beta} N^{\alpha\beta} d\Omega + \int_{\Omega} \delta\kappa_{\alpha\beta} M^{\alpha\beta} d\Omega \\
& - \int_{\Gamma_t} \delta\mathbf{v} \cdot \bar{\mathbf{t}} d\Gamma + \int_{\Gamma_M} \delta\mathbf{v}_{,\gamma} n^\gamma \mathbf{a}_3 M_{nn} d\Gamma + (\delta\mathbf{v} \cdot \mathbf{a}_3 P)_{\mathbf{x} \in C_P} - \int_{\Omega} \delta\mathbf{v} \cdot \bar{\mathbf{b}} d\Omega \\
& - \int_{\Gamma_v} \delta\mathbf{v} \cdot \mathbf{t} d\Gamma + \int_{\Gamma_\theta} \delta\theta_n M_{nn} d\Gamma + (\mathbf{v} \cdot \mathbf{a}_3 P)_{\mathbf{x} \in C_v} \\
& - \int_{\Gamma_v} \delta\mathbf{t} \cdot (\mathbf{v} - \bar{\mathbf{v}}) d\Gamma + \int_{\Gamma_\theta} \delta M_{nn} (\theta_n - \bar{\theta}_n) d\Gamma + (\delta P \mathbf{a}_3 \cdot (\mathbf{v} - \bar{\mathbf{v}}))_{\mathbf{x} \in C_v} \\
& + \sum_{i=1}^3 \alpha_{vi} \int_{\Gamma_v} (\delta\mathbf{v} \cdot \mathbf{a}_i) (\mathbf{a}_i \cdot \mathbf{v}) d\Gamma + \alpha_\theta \int_{\Gamma_\theta} \delta\theta_n \theta_n d\Gamma + \alpha_C (\delta\mathbf{v} \cdot \mathbf{a}_3 \mathbf{a}_3 \cdot \mathbf{v})_{\mathbf{x} \in C_v} \\
& \equiv 0
\end{aligned} \tag{57}$$

313

in which α_v , α_θ and α_C represent experimental artificial parameters. Further invoking the conventional reproducing kernel approximation of Eq. (22) leads to the following discrete equilibrium equations:

$$\sum_{J=1}^{n_p} (\mathbf{K}_{IJ} + \mathbf{K}_{IJ}^c + \mathbf{K}_{IJ}^s) \mathbf{d}_J = \mathbf{f}_I + \mathbf{f}^c + \mathbf{f}^s \tag{58}$$

316

where the stiffness \mathbf{K}_{IJ} is identical with Eq. (53). \mathbf{K}_{IJ}^c and \mathbf{K}_{IJ}^s are the stiffness matrices for consistent and stabilized terms, respectively, and have the following form:

$$\begin{aligned}
\mathbf{K}_{IJ}^c &= - \int_{\Gamma_v} (\Psi_I \mathbf{T}_{NJ} + \mathbf{T}_{NJ} \Psi_J) d\Gamma \\
&+ \int_{\Gamma_\theta} (\Psi_{I,\gamma} n^\gamma \mathbf{a}_3 M_{nnJ} + \mathbf{a}_3 M_{nnI} \Psi_{I,\gamma} n^\gamma) d\Gamma \\
&+ ([[\Psi_I \mathbf{a}_3 \mathbf{P}_J]]] + [[\mathbf{P}_I \mathbf{a}_3 \Psi_J]])_{\mathbf{x} \in C_v}
\end{aligned} \tag{59a}$$

$$\mathbf{f}_I^c = - \int_{\Gamma_v} \mathbf{T}_I \cdot \bar{\mathbf{v}} d\Gamma + \int_{\Gamma_\theta} M_{nnI} \bar{\theta}_n d\Gamma + [[\mathbf{P}_I \mathbf{a}_3 \cdot \bar{\mathbf{v}}]]_{\mathbf{x} \in C_v} \tag{59b}$$

319

$$\begin{aligned}
\mathbf{K}_{IJ}^s &= \alpha_v \int_{\Gamma_v} \Psi_I \Psi_J \mathbf{1} d\Gamma + \alpha_\theta \int_{\Gamma_\theta} \Psi_{I,\eta} n^\eta \mathbf{a}_3 \mathbf{a}_3 n^\gamma \Psi_{J,\gamma} d\Gamma + \alpha_C [[\Psi_I \mathbf{a}_3 \mathbf{a}_3 \Psi_J]]_{\mathbf{x} \in C_v} \\
\mathbf{f}_I^s &= \alpha_v \int_{\Gamma_v} \Psi_I \bar{\mathbf{v}} d\Gamma + \alpha_\theta \int_{\Gamma_\theta} \Psi_{I,\eta} n^\eta \mathbf{a}_3 \bar{\theta}_n d\Gamma + \alpha_C [[\Psi_I \mathbf{a}_3 \mathbf{a}_3 \cdot \bar{\mathbf{v}}]]_{\mathbf{x} \in C_v}
\end{aligned}$$

$$\tilde{\mathbf{K}}_{IJ}^s = \alpha_v \int_{\Gamma_v} \Psi_I \Psi_J d\Gamma + \alpha_\theta \int_{\Gamma_\theta} \Psi_{I,\eta} n^\eta \mathbf{a}_3 \mathbf{a}_3 n^\gamma \Psi_{J,\gamma} d\Gamma + \alpha_C [[\Psi_I \mathbf{a}_3 \mathbf{a}_3 \Psi_J]]_{\mathbf{x} \in C_v} \quad (60a)$$

$$\tilde{\mathbf{f}}_I^s = \alpha_v \int_{\Gamma_v} \Psi_I \bar{\mathbf{v}} d\Gamma + \alpha_\theta \int_{\Gamma_\theta} \Psi_{I,\eta} n^\eta \mathbf{a}_3 \bar{\theta}_n d\Gamma + \alpha_C [[\Psi_I \mathbf{a}_3 \mathbf{a}_3 \cdot \bar{\mathbf{v}}]]_{\mathbf{x} \in C_v} \quad (60b)$$

321 with

$$\alpha_v = \begin{bmatrix} \alpha_{v1} & 0 & 0 \\ 0 & \alpha_{v2} & 0 \\ 0 & 0 & \alpha_{v3} \end{bmatrix} \quad (61)$$

322 On comparing with the consistent terms of Eqs. (54) and (59), the expres-
 323 sions were almost identical, the major difference is that the higher order deriva-
 324 tives of shape functions have been replaced by smoothed gradients. Owing to
 325 the reproducing kernel framework, the construction of smoothed gradients only
 326 concerned about the computation of traditional meshfree shape functions and
 327 their first order derivatives, which avoid the costly computation of higher or-
 328 der derivatives. Moreover, the stabilized terms in Eq. (60) employs the penalty
 329 method with big enough artificial parameters to ensure the coercivity of stiffness.
 330 And the optimal values of these artificial parameters are proportional to the
 331 grid size of discrete model that can be represented by support size in meshfree
 332 approximation, where the $\alpha_{v1} \propto s^{-1}$, $\alpha_{v2} \propto s^{-3}$, $\alpha_\theta \propto s^{-1}$, $\alpha_C \propto s^{-2}$ [30], and
 333 $s = \min\{s_{all}\}$. In contrast, the stabilized term of Eq. (55) naturally exists in
 334 its weak form, and can stabilize the result without considering any artificial
 335 parameters.

336 **5. Numerical examples**

337 The suggested method, which uses Nitsche's method, the consistent repro-
 338 ducing kernel gradient smoothing integration scheme (RKGSI), and the non-
 339 consistent Gauss integration scheme (GI) with penalty method, as well as the
 340 proposed Hu-Washizu formulation (HW) to enforce the necessary boundary con-
 341 ditions, is validated in this section through several examples. A normalized
 342 support size of 2.5 is used for all the methods to ensure the requirement of
 343 quadratic base meshfree approximation. To eliminate the influence of integra-
 344 tion, the Gauss integration scheme uses 6 Gauss points for domain integration
 345 and 3 points for boundary integration, so as to maintain the same integration
 346 accuracy between domain and boundaries. Moreover, the number of integra-
 347 tion points are identical between the Gauss and RKGSI schemes. The error
 348 estimates of displacement (L_2 -Error) and energy (H_e -Error) is used here:

$$L_2\text{-Error} = \frac{\sqrt{\int_{\Omega}(\mathbf{v} - \mathbf{v}^h) \cdot (\mathbf{v} - \mathbf{v}^h) d\Omega}}{\sqrt{\mathbf{v} \cdot \mathbf{v}}}$$

$$H_e\text{-Error} = \frac{\sqrt{\int_{\Omega} \left((\varepsilon_{\alpha\beta} - \varepsilon_{\alpha\beta}^h)(N^{\alpha\beta} - N^{\alpha\beta h}) + \int_{\Omega} (\kappa_{\alpha\beta} - \kappa_{\alpha\beta}^h)(M^{\alpha\beta} - M^{\alpha\beta h}) \right) d\Omega}}{\sqrt{\int_{\Omega} (\varepsilon_{\alpha\beta} N^{\alpha\beta} + \kappa_{\alpha\beta} M^{\alpha\beta}) d\Omega}}$$
(62)

349 *5.1. Patch tests*

350 The linear and quadratic patch tests for flat and curved thin shells are firstly
 351 studied to verify the variational consistency of the proposed method. As shown
 352 in Fig. 3, the flat and curved models are depicted by an identical paramet-
 353 ric domain $\Omega = (0, 1) \otimes (0, 1)$, where the cylindrical coordinate system with
 354 radius $R = 1$ is employed to describe the curved model, and the whole do-
 355 main Ω is discretized by the 165 meshfree nodes. The artificial parameters
 356 of $\alpha_v = 10^5, \alpha_\theta = 10^3, \alpha_C = 10^5$ and $\alpha_v = 10^9, \alpha_\theta = 10^9, \alpha_C = 10^9$ are used for
 357 Nitsche's method and penalty method respectively. All the boundaries are en-
 358 forced as essential boundary conditions with the following manufactured exact
 359 solution:

$$\mathbf{v} = \begin{cases} (\xi^1 + 2\xi^2)^n \\ (3\xi^1 + 4\xi^2)^n \\ (5\xi^1 + 6\xi^2)^n \end{cases}, \quad n = \begin{cases} 1 & \text{Linear patch test} \\ 2 & \text{Quadratic patch test} \end{cases}$$
(63)

360 Table 1 lists the L_2 - and H_e -Error results of patch test with flat model, where
 361 the RKGSI scheme with variational consistent essential boundary enforcement,
 362 i.e. RKGSI-Nitsche and RKGSI-HW, can pass the linear and quadratic patch
 363 test. In contrast, the RKGSI-Penalty cannot pass the patch test since the
 364 Penalty method is unable to ensure the variational consistency. Due to the
 365 loss of variational consistency condition, even with Nitsche's method, Gauss
 366 meshfree formulations show noticeable errors. Table 2 shows the results for

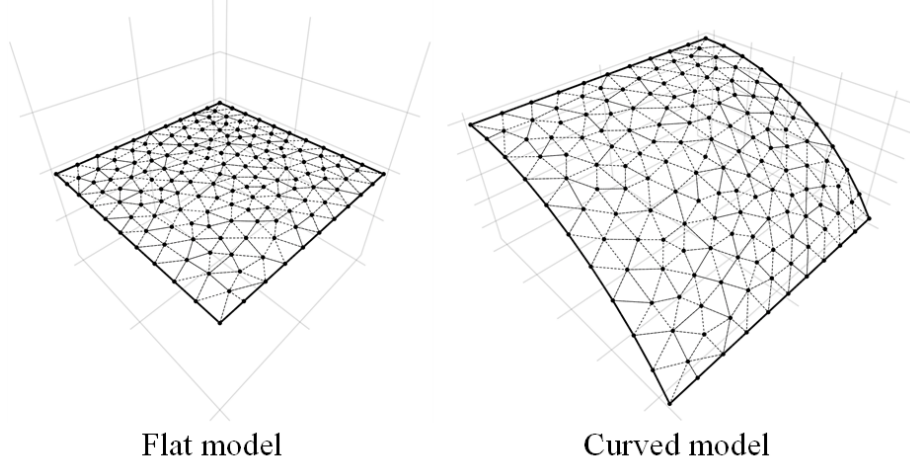


Figure 3: Meshfree discretization for patch test

367 curved model, which indicated that all the considered methods cannot pass the
 368 patch test. This is mainly because the proposed smoothed gradient of Eqs.
 369 (35) and (36) could not exactly reproduce the non-polynomial membrane and
 370 bending stress. However, the RKGSI-HW and RKGSI-Nitsche methods also
 371 provide better accuracy compared to others due to the fulfillment of first second-
 372 order variational consistency. And, even only with local variational consistency,
 373 the RKGSI-Penalty obtained a better result than traditional Gauss scheme.
 374 Meanwhile, the bending moment contours of M^{12} are listed in Fig. 4, which
 375 further verify that the proposed method provided a satisfactory result compared
 376 to exact solution. On the other hand, the RKGSI-Penalty and the conventional
 377 Gauss meshfree formulations showed errors.

Table 1: Results of patch test for flat model.

	Linear patch test		Quadratic patch test	
	L_2 -Error	H_e -Error	L_2 -Error	H_e -Error
GI-Penalty	$4.45E - 4$	$1.35E - 2$	$2.01E - 3$	$1.63E - 2$
GI-Nitsche	$4.51E - 4$	$1.42E - 2$	$1.22E - 3$	$1.68E - 2$
RKGSI-Penalty	$3.64E - 9$	$6.77E - 8$	$4.54E - 9$	$6.57E - 8$
RKGSI-Nitsche	$3.31E - 12$	$1.34E - 11$	$5.98E - 12$	$1.21E - 11$
RKGSI-HR	$6.67E - 13$	$1.50E - 11$	$1.07E - 12$	$1.26E - 11$

378 5.2. Scordelis-Lo roof

379 This example considers the classical Scordelis-Lo roof problem, as depicted
 380 in Fig. 5. The cylindrical roof has dimensions $R = 25$, $L = 50$, $h = 0.25$,
 381 Young's modulus $E = 4.32 \times 10^8$ and Poisson's ratio $\nu = 0.0$. The entire roof

Table 2: Results of patch test for cylindrical model.

	Linear patch test		Quadratic patch test	
	L_2 -Error	H_e -Error	L_2 -Error	H_e -Error
GI-Penalty	$3.79E - 4$	$1.30E - 2$	$1.74E - 3$	$1.37E - 2$
GI-Nitsche	$4.04E - 4$	$1.42E - 2$	$1.15E - 3$	$1.49E - 2$
RKGSI-Penalty	$1.47E - 4$	$5.39E - 3$	$2.26E - 4$	$2.09E - 3$
RKGSI-Nitsche	$2.41E - 6$	$7.37E - 5$	$2.47E - 6$	$2.89E - 5$
RKGSI-HR	$4.28E - 6$	$1.30E - 4$	$9.69E - 6$	$2.41E - 4$

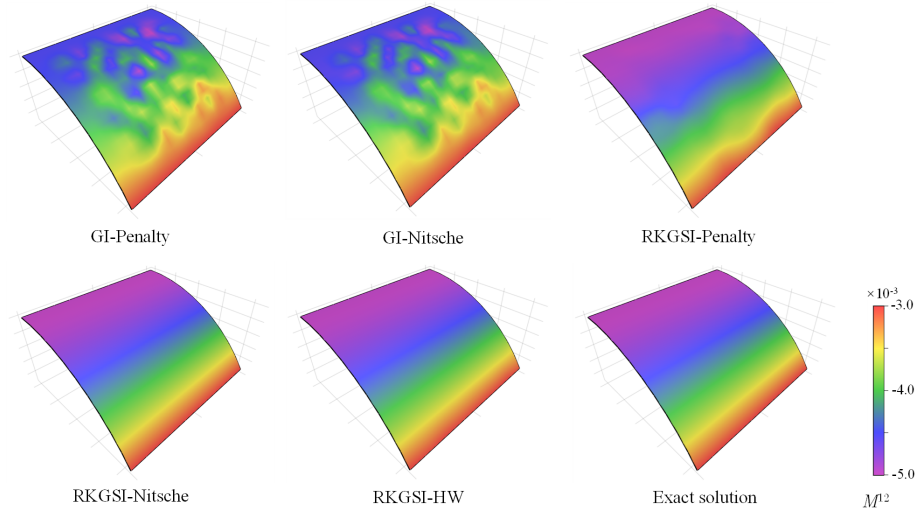


Figure 4: Contour plots of M^{12} for curved shell patch test.

is subjected to an uniform body force of $b_z = -90$, with the straight edges remainning free and the the curved edges are enforced by $v_x = v_z = 0$.

Due to the symmetry, only a quadrant of the model is considered for meshfree analysis, which is discretized by the 11×16 , 13×20 , 17×24 and 19×28 meshfree nodes, as listed in Fig. 6. The comparison of the displacement in z -direction at node A , v_{A3} , is used as the investigated quantity, with the reference value 0.3024 given by [33] 0.3006 given by [34]. Firstly, Fig. 7 presents a sensitivity study for the artificial parameters of α_v 's, α_{v3} 's and α_θ 's in the RKGSI meshfree formulations with Nitsche's method and penalty method— where all of the parameters are scaled by the support size as, $\alpha_{v0} = s^{-1}\bar{\alpha}_v$, $\alpha_{v3} = s^{-3}\bar{\alpha}_v$ and $\alpha_\theta = s^{-1}\bar{\alpha}_\theta$. For a better comparison, the result of proposed RKGSI-HW is also listed in this figure. The results of Fig. 7 revealed, Nitsche's method observed less artificial sensitivity. However, both the methods cannot trivially determine the optimal values of the artificial parameters. The optimal artificial parameters from Fig. 7 are adopted for the convergence study in Fig. 8. The

³⁹⁷ convergence result showed that the RKGSI get satisfactory results while the
³⁹⁸ traditional Gauss methods demonstrated noticeable errors.

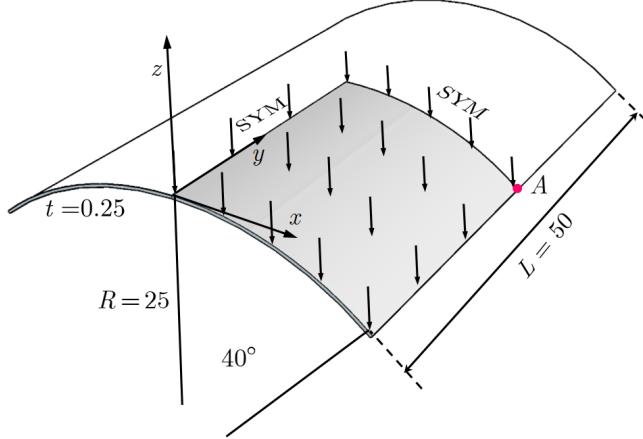


Figure 5: Description of Scordelis-Lo roof problem.

³⁹⁹ 5.3. Pinched Hemispherical shell

⁴⁰⁰ Consider the hemispherical shell shown in Fig. 9, which is loaded at four
⁴⁰¹ points $P = \pm 2$ at 90° interval at its bottom. The hemispherical shell has an
⁴⁰² radius $R = 10$, thickness $h = 0.04$, Young's modulus $E = 6.825 \times 10^7$ and
⁴⁰³ Poisson's ratio $\nu = 0.3$.

⁴⁰⁴ Due to symmetry, only quadrant model, where the ~~8 × 8, 16 × 16, 24 × 24~~ and
⁴⁰⁵ ~~32 × 32 and 40 × 40~~ meshfree nodes have been discretized as shown in Fig.
⁴⁰⁶ (10), was considered. The quantity under investigation for convergence is the
⁴⁰⁷ displacement at x -direction on point A , v_{A1} . Fig. 11 displays the correspond-
⁴⁰⁸ ing convergence results, indicating the RKGSI scheme performed significantly
⁴⁰⁹ better compared to the GI meshfree formulation. Meanwhile, the efficiency
⁴¹⁰ comparison for this problem is also shown in Fig. 12, in which the CPU time
⁴¹¹ for assembly and calculation of shape functions are considered. Fig. 12(a) indi-
⁴¹² cates that the RKGSI scheme observed high efficiency in assembly. This is due
⁴¹³ to the variational inconsistent Gauss meshfree formulation which require more
⁴¹⁴ Gaussian points to get satisfactory results. Fig. 12(b) lists the CPU time spent
⁴¹⁵ on enforcing essential boundary conditions for the penalty method, Nitsche's
⁴¹⁶ method and proposed HW method. The results highlighted that the proposed
⁴¹⁷ HW method consumed comparable CPU time in assembly compared to Nitsche's
⁴¹⁸ method. However, less time was spent to calculate the shape functions. Since
⁴¹⁹ both the HW method and penalty method were developed considering the shape
⁴²⁰ functions first order derivatives. For this reason, both the methods shared an
⁴²¹ almost identical time in computing the shape functions.

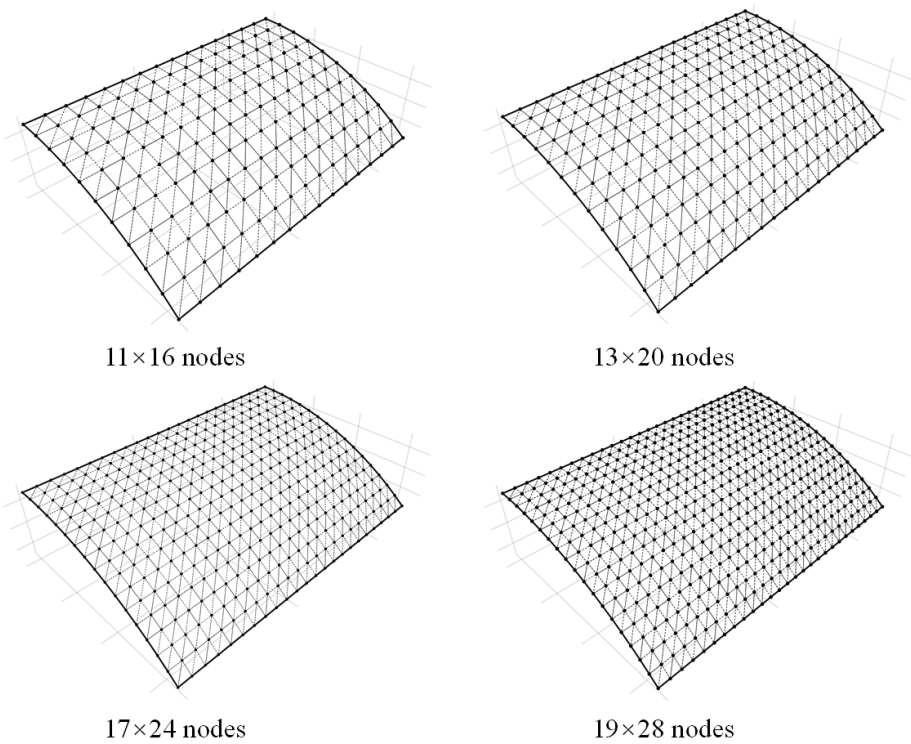


Figure 6: Meshfree discretizations for Scordelis-Lo roof problem.

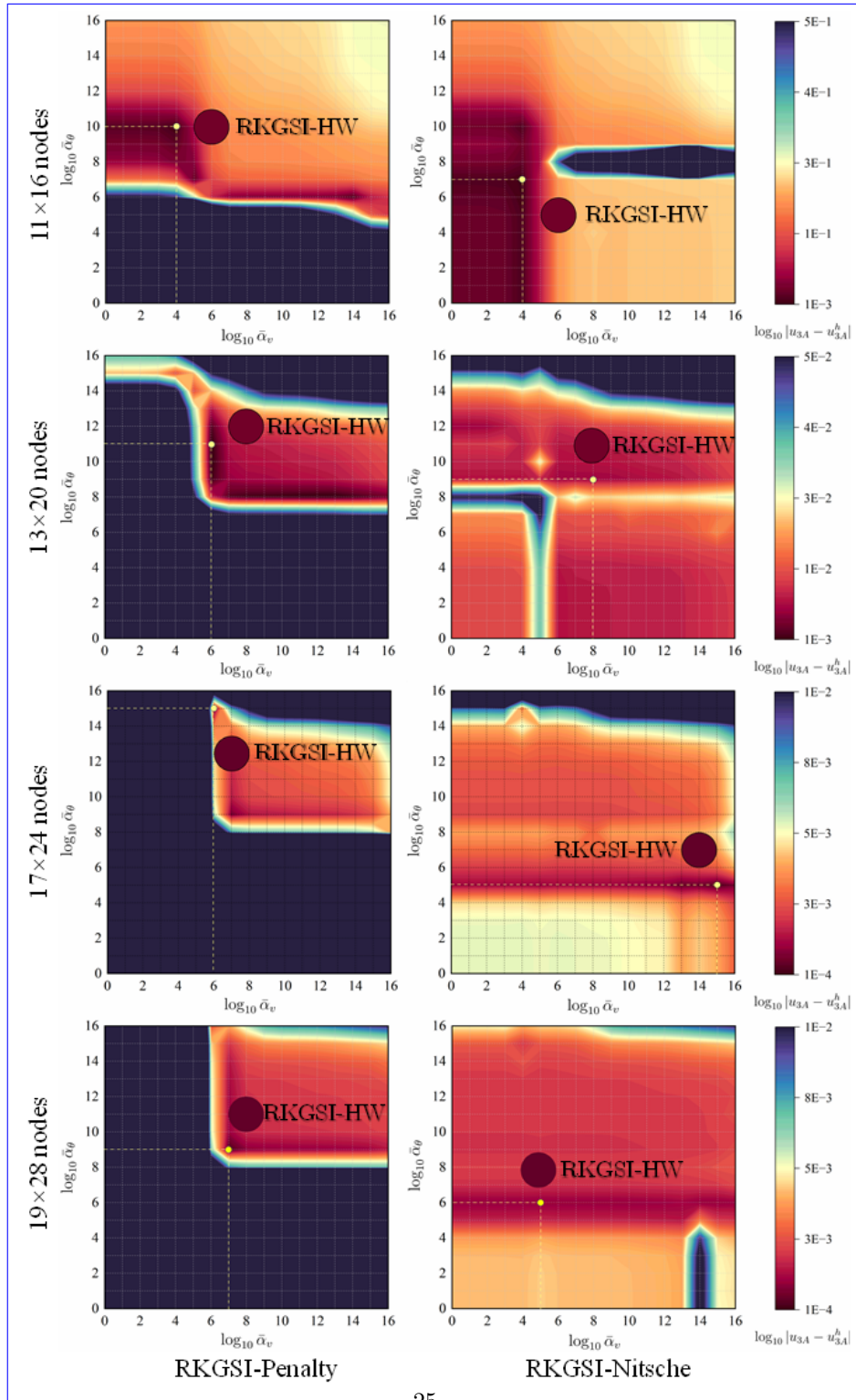


Figure 7: Sensitivity comparison of α_v and α_θ for Scordelis-Lo problem.

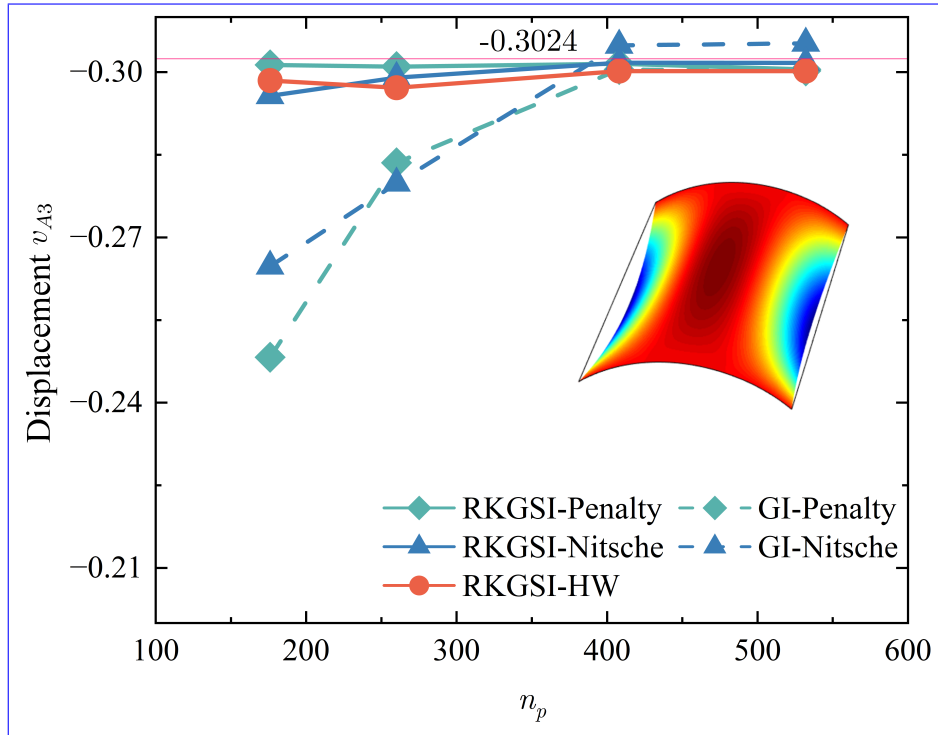


Figure 8: Displacement convergence for Scordelis-Lo roof problem.

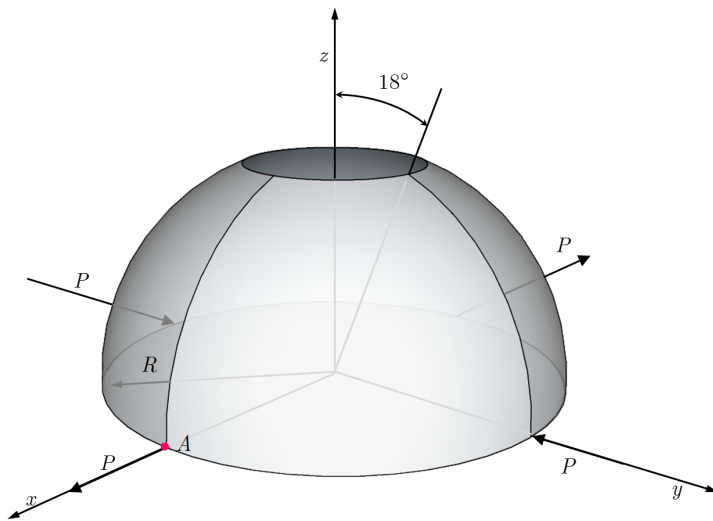


Figure 9: Description of pinched hemispherical shell problem.

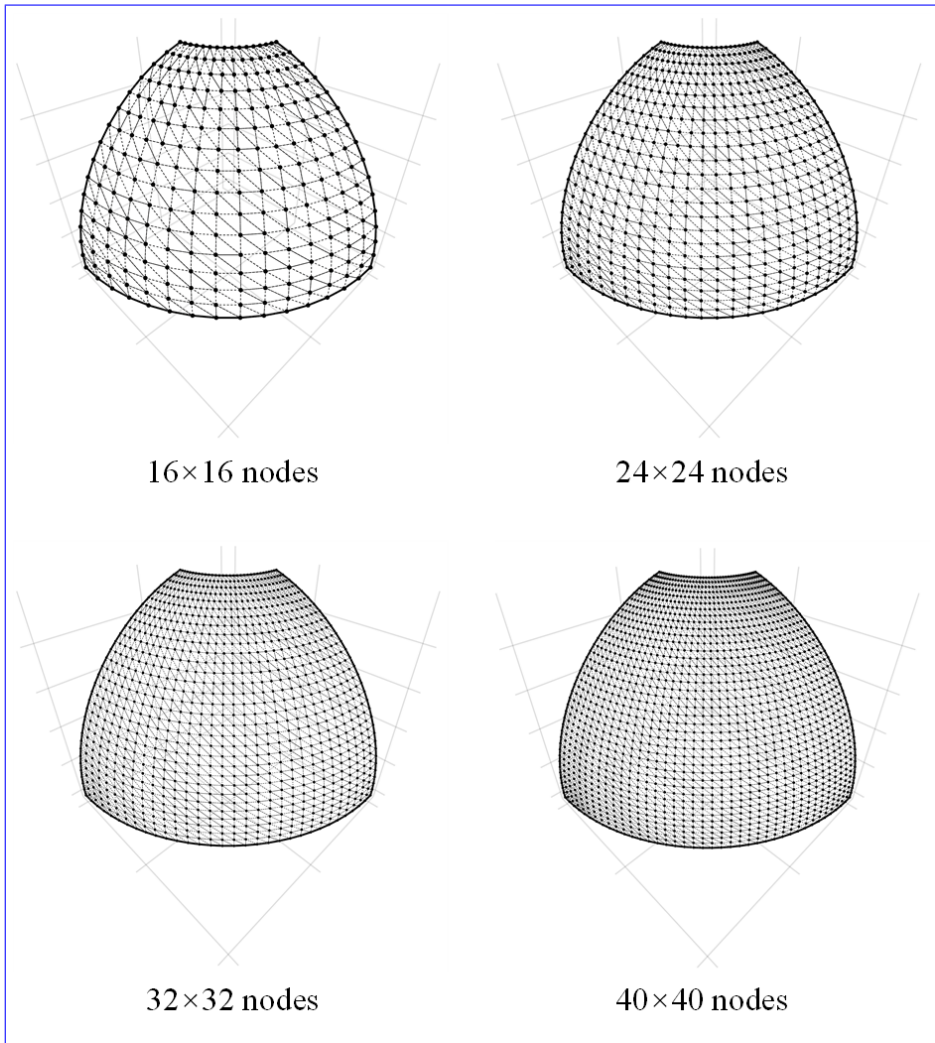


Figure 10: [Meshfree discretizations for pinched hemispherical shell problem.](#)

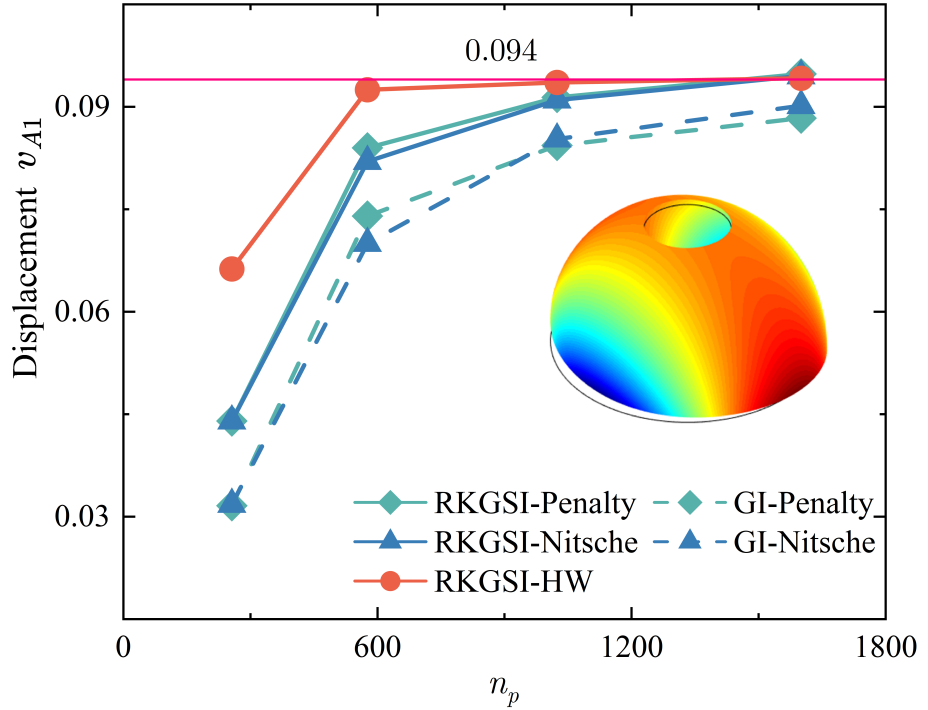


Figure 11: Displacement convergence for pinched hemispherical shell problem.

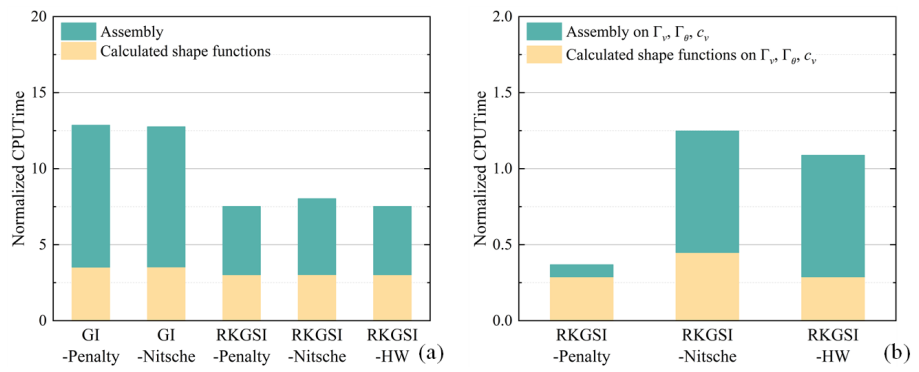


Figure 12: efficiency comparison for pinched hemispherical shell problem: (a) Whole domain; (b) Essential boundaries

422 **6. Conclusion**

423 In this study, an efficient and quasi-consistent meshfree thin shell formu-
424 lation was presented to naturally enforce the essential boundary conditions.
425 Mixed formulation with the Hu-Washizu principle weak form is adopted, where
426 the traditional meshfree shape functions discretized the displacement, and the
427 strains and stresses were expressed by the reproducing kernel smoothed gradi-
428 ents and the covariant smoothed gradients, respectively. The smoothed gradient
429 naturally embedded the first second-order integration constraints and has
430 a quasi variational consistency for the curved models in each integration cell.
431 Owing to the Hu-Washizu variational principle, the essential boundary condi-
432 tion enforcement has a similar form with the conventional Nitsche's method;
433 both have consistent and stabilized terms. The costly high order derivatives
434 in the Nitsche's consistent term have been replaced by the smoothed gradients,
435 which improved the computational speed due to the reproducing kernel gradient
436 smoothing framework. Furthermore, the stabilized term naturally existed in the
437 Hu-Washizu weak form, and the artificial parameter needed in Nitsche's stabi-
438 lized term has vanished, which can automatically maintain the coercivity for
439 the stiffness matrix. Based on general reproducing kernel gradient smoothing
440 framework, the proposed methodology can be trivially extended to high order
441 basis meshfree formulation. The numerical results demonstrated that the pro-
442 posed Hu-Washizu quasi-consistent meshfree thin shell formulation showed ex-
443 cellent accuracy, efficiency, and stability.

⁴⁴⁴ **Acknowledgment**

⁴⁴⁵ The support of this work by the National Natural Science Foundation of
⁴⁴⁶ China (12102138, 52350410467) and the Natural Science Foundation of Fujian
⁴⁴⁷ Province of China (2023J01108, 2022J05056) is gratefully acknowledged.

448 **Appendix A. Green's theorems for in-plane vector**

449 This Appendix discusses two kinds of Green's theorems used for the development
 450 of the proposed meshfree method. For an arbitrary vectors v^α and a
 451 scalar function f , with Green's theorem for in-plane vector, the first Green's
 452 theorem is listed as follows [30]:

$$\begin{aligned} \int_{\Omega} f_{,\alpha} v^\alpha d\Omega &= \int_{\Gamma} f v^\alpha n_\alpha d\Gamma - \int_{\Omega} f(v_{,\alpha}^\alpha + \Gamma_{\beta\alpha}^\beta v^\alpha) d\Omega \\ &= \int_{\Gamma} f v^\alpha n_\alpha d\Gamma - \int_{\Omega} f v^\alpha|_\alpha d\Omega \end{aligned} \quad (\text{A.1})$$

453 where $\Gamma_{\alpha\beta}^\gamma = \mathbf{a}_{\alpha,\beta} \cdot \mathbf{a}^\gamma$ denotes the Christoffel symbol of the second kind. $v^\alpha|_\alpha$
 454 can be represented as the in-plane covariant derivative of the vector v^α :

$$v^\alpha|_\alpha = v_{,\alpha}^\alpha + \Gamma_{\beta\alpha}^\beta v^\alpha \quad (\text{A.2})$$

455 The second Green's theorem is established with a mixed form of second
 456 order derivative. Let $A^{\alpha\beta}$ can be an arbitrary symmetric second order tensor,
 457 the Green's theorem yields [30]:

$$\begin{aligned} \int_{\Omega} f_{,\alpha}|_\beta A^{\alpha\beta} d\Omega &= \int_{\Gamma} f_{,\gamma} n^\gamma A^{\alpha\beta} n_\alpha n_\beta d\Gamma - \int_{\Gamma} f(A^{\alpha\beta} s_\alpha n_\beta)_{,\gamma} s^\gamma d\Gamma + [[f A^{\alpha\beta} s_\alpha n_\beta]]_{\mathbf{x}\in C} \\ &\quad - \int_{\Gamma} f(A_{,\beta}^{\alpha\beta} n_\alpha + \Gamma_{\alpha\beta}^\gamma A^{\alpha\beta} n_\gamma + \Gamma_{\gamma\beta}^\gamma A^{\alpha\beta} n_\alpha) d\Gamma \\ &\quad + \int_{\Omega} f \left(\begin{array}{l} \Gamma_{\alpha\beta,\gamma}^\gamma A^{\alpha\beta} + \Gamma_{\alpha\beta}^\gamma A^{\alpha\beta} + \Gamma_{\eta\gamma}^\eta \Gamma_{\alpha\beta}^\gamma A^{\alpha\beta} \\ + A_{,\alpha\beta}^{\alpha\beta} + \Gamma_{\gamma\beta,\alpha}^\gamma A^{\alpha\beta} + 2\Gamma_{\gamma\alpha}^\gamma A_{,\beta}^{\alpha\beta} + \Gamma_{\gamma\alpha}^\gamma \Gamma_{\eta\beta}^\eta A^{\alpha\beta} \end{array} \right) d\Omega \\ &= \int_{\Gamma} f_{,\gamma} n^\gamma A^{\alpha\beta} n_\alpha n_\beta d\Gamma - \int_{\Gamma} f(A^{\alpha\beta} s_\alpha n_\beta)_{,\gamma} s^\gamma d\Gamma + [[f A^{\alpha\beta} s_\alpha n_\beta]]_{\mathbf{x}\in C} \\ &\quad - \int_{\Gamma} f A^{\alpha\beta}|_\beta n_\alpha d\Gamma + \int_{\Omega} f A^{\alpha\beta}|_\alpha n_\beta d\Omega \end{aligned} \quad (\text{A.3})$$

458 with

$$A^{\alpha\beta}|_\beta = A_{,\beta}^{\alpha\beta} + \Gamma_{\beta\gamma}^\alpha A^{\beta\gamma} + \Gamma_{\gamma\beta}^\gamma A^{\alpha\beta} \quad (\text{A.4})$$

$$\begin{aligned} A^{\alpha\beta}|_{\alpha\beta} &= \Gamma_{\alpha\beta,\gamma}^\gamma A^{\alpha\beta} + \Gamma_{\alpha\beta}^\gamma A^{\alpha\beta} + \Gamma_{\eta\gamma}^\eta \Gamma_{\alpha\beta}^\gamma A^{\alpha\beta} \\ &\quad + A_{,\alpha\beta}^{\alpha\beta} + \Gamma_{\gamma\beta,\alpha}^\gamma A^{\alpha\beta} + 2\Gamma_{\gamma\alpha}^\gamma A_{,\beta}^{\alpha\beta} + \Gamma_{\gamma\alpha}^\gamma \Gamma_{\eta\beta}^\eta A^{\alpha\beta} \end{aligned} \quad (\text{A.5})$$

460 For the sake of brevity, the notion of covariant derivative is extended to a
 461 scalar function as:

$$f|_\alpha = f_{,\alpha} + \Gamma_{\beta\alpha}^\beta f \quad (\text{A.6})$$

$$f|_\beta n_\alpha = f_{,\beta} n_\alpha + \Gamma_{\alpha\beta}^\gamma f n_\gamma + \Gamma_{\gamma\beta}^\gamma f n_\alpha \quad (\text{A.7})$$

$$\begin{aligned} f|_{\alpha\beta} &= \Gamma_{\alpha\beta,\gamma}^\gamma f + \Gamma_{\alpha\beta}^\gamma f_{,\gamma} + \Gamma_{\eta\gamma}^\eta \Gamma_{\alpha\beta}^\gamma f \\ &\quad + f_{,\alpha\beta} + \Gamma_{\gamma\beta,\alpha}^\gamma f + 2\Gamma_{\gamma\alpha}^\gamma f_{,\beta} + \Gamma_{\gamma\alpha}^\gamma \Gamma_{\eta\beta}^\eta f \end{aligned} \quad (\text{A.8})$$

⁴⁶⁴ **Appendix B. Derivations for stiffness metrics and force vectors**

⁴⁶⁵ This Appendix details the derivations of stiffness matrices and force vectors
⁴⁶⁶ in Eqs. (53)-(55), where the relationships of Eqs. (40), (41), (44) and (46) are
⁴⁶⁷ used herein. Firstly, the membrane strain terms are considered as follows:

$$\begin{aligned}
 & \sum_{C=1}^{n_e} \int_{\Omega_C} \delta \tilde{\varepsilon}_{\alpha\beta}^h h C^{\alpha\beta\gamma\eta} \tilde{\varepsilon}_{\gamma\eta}^h d\Omega \\
 &= \sum_{C=1}^{n_e} \sum_{I,J=1}^{n_p} \delta \mathbf{d}_I \cdot \underbrace{\int_{\Omega_C} \tilde{\varepsilon}_{\alpha\beta I} h C^{\alpha\beta\gamma\eta} \mathbf{a}_\gamma \mathbf{q}^T d\Omega \mathbf{G}^{-1} \bar{\mathbf{g}}_{\eta J} \cdot \mathbf{d}_J}_{\tilde{\mathbf{g}}_I^{\eta T}} \\
 &= \sum_{C=1}^{n_e} \sum_{I,J=1}^{n_p} \delta \mathbf{d}_I \cdot \int_{\Gamma_C \cap \Gamma_v} \Psi_J \underbrace{\mathbf{q}^T \mathbf{G}^{-1} \tilde{\mathbf{g}}_I^\alpha n_\alpha}_{\tilde{\mathbf{T}}_{NI}} d\Gamma \cdot \mathbf{d}_J \\
 &= \sum_{I,J=1}^{n_p} \delta \mathbf{d}_I \cdot \int_{\Gamma_v} \tilde{\mathbf{T}}_{NI} \Psi_J d\Gamma \cdot \mathbf{d}_J
 \end{aligned} \tag{B.1}$$

⁴⁶⁸ with

$$\tilde{\mathbf{g}}_I^\alpha = \mathbf{q} \mathbf{a}_\beta h C^{\alpha\beta\gamma\eta} \tilde{\varepsilon}_{\gamma\eta} \mathbf{a}_\beta \mathbf{q}^T \tag{B.2}$$

⁴⁶⁹

$$\tilde{\mathbf{T}}_{NI} = \mathbf{q}^T \mathbf{G}^{-1} \tilde{\mathbf{g}}_I^\alpha n_\alpha \tag{B.3}$$

⁴⁷⁰ Following this path, the bending strain terms can be reorganized by:

$$\begin{aligned}
 & \sum_{C=1}^{n_e} \int_{\Omega_C} \delta \tilde{\kappa}_{\alpha\beta}^h \frac{h^3}{12} C^{\alpha\beta\gamma\eta} \bar{\kappa}_{\gamma\eta}^h d\Omega \\
 &= \sum_{C=1}^{n_e} \sum_{I,J=1}^{n_p} \delta \mathbf{d}_I \cdot \underbrace{\int_{\Omega_C} \tilde{\kappa}_{\alpha\beta I} \frac{h^3}{12} C^{\alpha\beta\gamma\eta} \mathbf{a}_3 \mathbf{q}^T d\Omega \mathbf{G}^{-1} \bar{\mathbf{g}}_{\gamma\eta J} \cdot \mathbf{d}_J}_{\tilde{\mathbf{g}}_I^{\gamma\eta T}} \\
 &= \sum_{C=1}^{n_e} \sum_{I,J=1}^{n_p} \delta \mathbf{d}_I \cdot \left(\begin{array}{l} \int_{\Gamma_C \cap \Gamma_\theta} \underbrace{\mathbf{q}^T \mathbf{G}^{-1} \tilde{\mathbf{g}}_I^{\alpha\beta} n_\alpha n_\beta}_{\tilde{\mathbf{M}}_{nnI}} n^\gamma \Psi_{J,\gamma} d\Gamma \\ - \int_{\Gamma_C \cap \Gamma_v} \underbrace{(\mathbf{q}_{|\beta}^T \mathbf{G}^{-1} \tilde{\mathbf{g}}_I^{\alpha\beta} n_\alpha + (\mathbf{q}^T \mathbf{G}^{-1} \tilde{\mathbf{g}}_I^{\alpha\beta} s_\alpha n_\beta)_{,\gamma} s^\gamma)}_{\tilde{\mathbf{T}}_{MI}} \Psi_{J,\gamma} d\Gamma \\ + [[\underbrace{\mathbf{q}^T \mathbf{G}^{-1} \tilde{\mathbf{g}}_I^{\alpha\beta} s_\alpha n_\beta}_{\tilde{\mathbf{P}}_I \mathbf{a}_3} \Psi_J]]_{\mathbf{x} \in C_C \cap C_v} \end{array} \right) \cdot \mathbf{d}_J \\
 &= \sum_{I,J=1}^{n_p} \delta \mathbf{d}_I \cdot \left(\int_{\Gamma_\theta} \tilde{\mathbf{M}}_{nnI} n^\gamma \Psi_{J,\gamma} d\Gamma - \int_{\Gamma_v} \tilde{\mathbf{T}}_{MI} \Psi_{J,\gamma} d\Gamma + [[\tilde{\mathbf{P}}_I \Psi_J]]_{\mathbf{x} \in C_v} \right)
 \end{aligned} \tag{B.4}$$

⁴⁷¹ with

$$\tilde{\mathbf{g}}_I^{\alpha\beta} = \int_{\Omega_C} \mathbf{q} \frac{h^3}{12} C^{\alpha\beta\gamma\eta} \mathbf{a}_3 \tilde{\kappa}_{\underline{\gamma}\underline{\eta}\underline{I}\underline{\alpha}\underline{\beta}\underline{I}} d\Omega \quad (\text{B.5})$$

⁴⁷²

$$\begin{cases} \tilde{M}_{nnI} = \mathbf{q}^T \mathbf{G}^{-1} \tilde{\mathbf{g}}_I^{\alpha\beta} n_\alpha n_\beta \\ \tilde{T}_{MI} = \mathbf{q}_{|\beta}^T \mathbf{G}^{-1} \tilde{\mathbf{g}}_I^{\alpha\beta} n_\alpha + (\mathbf{q}^T \mathbf{G}^{-1} \tilde{\mathbf{g}}_I^{\alpha\beta} s_\alpha n_\beta)_{,\gamma} s^\gamma \\ \tilde{P}_I = \mathbf{q}^T \mathbf{G}^{-1} \tilde{\mathbf{g}}_I^{\alpha\beta} s_\alpha n_\beta \cdot \mathbf{a}_3 \end{cases} \quad (\text{B.6})$$

473 **References**

- 474 [1] L. H. Donnell, Beams, Plates and Shells, McGraw-Hill, 1976.
- 475 [2] T. J. Hughes, The Finite Element Method: Linear Static and Dynamic
476 Finite Element Analysis, Dover Publications, Mineola, New York, 2000.
- 477 [3] T. Belytschko, Y. Y. Lu, L. Gu, Element-free Galerkin methods, Interna-
478 tional Journal for Numerical Methods in Engineering 37 (1994) 229–256.
- 479 [4] W. K. Liu, S. Jun, Y. F. Zhang, Reproducing kernel particle methods,
480 International Journal for Numerical Methods in Fluids 20 (1995) 1081–
481 1106.
- 482 [5] J. S. Chen, M. Hillman, S. W. Chi, Meshfree methods: Progress made after
483 20 Years, Journal of Engineering Mechanics 143 (2017) 04017001.
- 484 [6] P. Krysl, T. Belytschko, Analysis of thin shells by the Element-Free
485 Galerkin method, International Journal of Solids and Structures 33 (1996)
486 3057–3080.
- 487 [7] G. R. Liu, Meshfree Methods: Moving Beyond the Finite Element Method,
488 Second Edition, Crc Press, 2009.
- 489 [8] D. Millán, A. Rosolen, M. Arroyo, Thin shell analysis from scattered points
490 with maximum-entropy approximants, International Journal for Numerical
491 Methods in Engineering 85 (2011) 723–751.
- 492 [9] L. Wang, M. Hu, Z. Zhong, F. Yang, Stabilized Lagrange Interpolation
493 Collocation Method: A meshfree method incorporating the advantages of
494 finite element method, Computer Methods in Applied Mechanics and En-
495 gineering 404 (2023) 115780.
- 496 [10] X. Zhang, K. Z. Song, M. W. Lu, X. Liu, Meshless methods based on
497 collocation with radial basis functions, Computational Mechanics 26 (2000)
498 333–343.
- 499 [11] P. Suchde, T. Jacquemin, O. Davydov, Point Cloud Generation for Mesh-
500 free Methods: An Overview, Archives of Computational Methods in Engi-
501 neering 30 (2022) 889–915.
- 502 [12] L. Deng, D. Wang, An accuracy analysis framework for meshfree collocation
503 methods with particular emphasis on boundary effects, Computer Methods
504 in Applied Mechanics and Engineering 404 (2023) 115782.
- 505 [13] J. Wang, M. Hillman, Upwind reproducing kernel collocation method for
506 convection-dominated problems, Computer Methods in Applied Mechanics
507 and Engineering 420 (2024) 116711.

- 508 [14] S. Fernández-Méndez, A. Huerta, Imposing essential boundary conditions
 509 in mesh-free methods, Computer Methods in Applied Mechanics and En-
 510 gineering 193 (2004) 1257–1275.
- 511 [15] X. Li, Error estimates for the moving least-square approximation and the
 512 element-free Galerkin method in n-dimensional spaces, Applied Numerical
 513 Mathematics 99 (2016) 77–97.
- 514 [16] J. Wu, D. Wang, An accuracy analysis of Galerkin meshfree methods ac-
 515 counting for numerical integration, Computer Methods in Applied Mechan-
 516 ics and Engineering 375 (2021) 113631.
- 517 [17] J. S. Chen, H. P. Wang, New boundary condition treatments in meshfree
 518 computation of contact problems, Computer Methods in Applied Mechan-
 519 ics and Engineering 187 (2000) 441–468.
- 520 [18] D. Liu, Y. M. Cheng, The interpolating element-free Galerkin (IEFG)
 521 method for three-dimensional potential problems, Engineering Analysis
 522 with Boundary Elements 108 (2019) 115–123.
- 523 [19] V. Ivannikov, C. Tiago, P. M. Pimenta, On the boundary conditions of the
 524 geometrically nonlinear Kirchhoff–Love shell theory, International Journal
 525 of Solids and Structures 51 (2014) 3101–3112.
- 526 [20] Y. Y. Lu, T. Belytschko, L. Gu, A new implementation of the element free
 527 Galerkin method, Computer Methods in Applied Mechanics and Engineer-
 528 ing 113 (1994) 397–414.
- 529 [21] T. Zhu, S. N. Atluri, A modified collocation method and a penalty formu-
 530 lation for enforcing the essential boundary conditions in the element free
 531 Galerkin method, Computational Mechanics 21 (1998) 211–222.
- 532 [22] S. Skatulla, C. Sansour, Essential boundary conditions in meshfree methods
 533 via a modified variational principle: Applications to shell computations,
 534 Computer Assisted Mechanics and Engineering Sciences 15 (2008) 123–142.
- 535 [23] J. S. Chen, C. T. Wu, S. Yoon, Y. You, A stabilized conforming nodal
 536 integration for Galerkin mesh-free methods, International Journal for Nu-
 537 merical Methods in Engineering 50 (2001) 435–466.
- 538 [24] J. S. Chen, M. Hillman, M. Rüter, An arbitrary order variationally consis-
 539 tent integration for Galerkin meshfree methods, International Journal for
 540 Numerical Methods in Engineering 95 (2013) 387–418.
- 541 [25] Q. Duan, X. Li, H. Zhang, T. Belytschko, Second-order accurate derivatives
 542 and integration schemes for meshfree methods, International Journal for
 543 Numerical Methods in Engineering 92 (2012) 399–424.

- 544 [26] D. Wang, J. Wu, An inherently consistent reproducing kernel gradient
 545 smoothing framework toward efficient Galerkin meshfree formulation with
 546 explicit quadrature, Computer Methods in Applied Mechanics and Engi-
 547 neering 349 (2019) 628–672.
- 548 [27] J. Wang, X. Ren, A consistent projection integration for Galerkin meshfree
 549 methods, Computer Methods in Applied Mechanics and Engineering 414
 550 (2023) 116143.
- 551 [28] J. Wu, X. Wu, Y. Zhao, D. Wang, A consistent and efficient method for
 552 imposing meshfree essential boundary conditions via hellinger-reissner vari-
 553 ational principle., Chinese Journal of Theoretical and Applied Mechanics
 554 54 (2022) 3283–3296.
- 555 [29] J. Wu, X. Wu, Y. Zhao, D. Wang, A rotation-free Hellinger-Reissner mesh-
 556 free thin plate formulation naturally accommodating essential boundary
 557 conditions, Engineering Analysis with Boundary Elements 154 (2023) 122–
 558 140.
- 559 [30] J. Benzaken, J. A. Evans, S. F. McCormick, R. Tamstorf, Nitsche’s method
 560 for linear Kirchhoff–Love shells: Formulation, error analysis, and verifica-
 561 tion, Computer Methods in Applied Mechanics and Engineering 374 (2021)
 562 113544.
- 563 [31] H. Dah-wei, A method for establishing generalized variational principle,
 564 Applied Mathematics and Mechanics 6 (1985) 501–509.
- 565 [32] H. Du, J. Wu, D. Wang, J. Chen, A unified reproducing kernel gradient
 566 smoothing Galerkin meshfree approach to strain gradient elasticity, Com-
 567 putational Mechanics 70 (2022) 73–100.
- 568 [33] R. H. MacNeal, R. L. Harder, A proposed standard set of problems to test
 569 finite element accuracy, Finite Elements in Analysis and Design 1 (1985)
 570 3–20.
- 571 [34] J. Kiendl, K. U. Bletzinger, J. Linhard, R. Wüchner, Isogeometric shell
 572 analysis with Kirchhoff–Love elements, Computer Methods in Applied Me-
 573 chanics and Engineering 198 (2009) 3902–3914.